MAJOR QUALIFYING PROJECT

as a partial requirement
for

BACHELOR OF SCIENCE
MECHANICAL ENGINEERING
MECHANICAL DESIGN CONCENTRATION

REPORT:

LINEAR CAM DESIGN FOR PRODUCT ALIGNMENT

Submitted by:

_____
Matthias Downey; mpdowney@wpi.edu

_____
Peter Holmes; pjholm28@wpi.edu

_____
Joseph Mayo; joemayo@wpi.edu

_____
Christopher Wells; cwells@wpi.edu

Submitted to:

_____
Professor Robert L. Norton

DEPARTMENT OF MECHANICAL ENGINEERING
WORCESTER POLYTECHNIC INSTITUTE
WORCESTER, MA 01609-2280

December 17, 2009

Acknowledgements

Prof. Robert L. Norton, P.E.

Project Advisor

Corey Maynard

Project Liaison

Kenneth Belliveau

Project Liaison

Jeffery Kittredge

Project Liaison

Charles Gillis

Engineer

David Clancy

Engineer

Ernest Chandler

High Speed Video

Adam Lane

Mechanic Supervisor

Mike McGourthy

Mechanic

Larry Clinton

Mechanic

Toan Nguyen

Prototype Lab

Dan Labelle

Prototype Inspection

Mike Cavalier

Prototype Mechanic

Abstract

A high-output, automated machine assembles two components, contacting one component against carbide stops for locating purposes. The contact forces are sufficient to locally yield the material. This project entails the design of a linear cam mechanism that gently aligns this component on an existing station without causing any yielding. We created a dynamic simulation of two cam trains, which we used as a design basis after verification against measured data. As a sub-project, we redesigned one of the existing cams to reduce a large spike of acceleration at a deliberate impact that we noticed in our measured data.

Executive Summary

The assembly of many consumer products is completed on indexing, automatic assembly machines in large factories. Large scale raw materials and pre-fabricated parts are fed into these machines and automatic processes create assemblies, check for quality control and send out the parts to another step in the process. A certain indexing, automatic assembly machine combines Part A and Part B together and outputs the resultant product. Part A is aligned and placed on top of Part B on an indexing nest. The two parts are fastened together, inspected for consistency, and output to another process.

The problem presented to us by our sponsor is that the current alignment method relies on a mechanism pushing on the backside of Part A, pushing the opposite edge into carbide stops to locate it accurately with respect to Part B. The contact forces are sufficient to locally yield the material and cause a small permanent deformation of a few thousandths of an inch. This process is unfavorable for several reasons including a possible decrease in placement accuracy and excess material from the "crush" causing interference during the feeding process of subsequent machine in the process. The suggested modification was to reverse this process and move it outside of the fastening box to the Part A placement station, just prior to the fastening station.

In addition to the loading problems in subsequent processes caused by the deformed edge, the contacting mechanism is in a sealed off box immediately prior to joining the two parts. This box is difficult to access for repairs and it limits the ability to make modifications.

The goal of our project was to provide our sponsor with a method to accurately locate Part A on top of Part B prior to fastening without locally deforming Part A. We achieved this goal by completing the following objectives:

- Analyzed and interpreted the existing process to determine what changes are feasible within the process.
- Designed a linear cam to gently close the nest jaw, accurately pushing Part A to a known location before fastening to Part B.
- Redesigned the transfer cam to reduce the violent impact collision between the slice bar and the hard stop. We added this objective after noticing a very large impact force in our analysis.

Analysis

Before attempting to redesign any part of the product assembly machine, we analyzed the existing transfer station. We modeled both of the cam trains involved in the placement of Part A on top of Part B. Using a lumped mass model, we determined an effective overall spring constant and an effective mass for each cam train. These constants were input into Program Dynacam to create a dynamic simulation of the displacement, velocity, and acceleration of each cam train. This simulation was then converted to g's and compared to accelerometer data, measured on the running machine at each end effecter, to determine the validity of our model. Figure 1 (a) shows this comparison for the lift cam, while Figure 1 (b) shows this comparison for the transfer cam. We calculated moving averages to smooth the electrical and mechanical noise. Both comparisons show impact spikes, which were caused by shot pin insertion for the lift cam and by an impact with a hard stop for the transfer cam. Figure 1 (b) shows the impact spike truncated at 15 g's; however, this impact spike reaches 48 g's, which inspired us to redesign the transfer cam to reduce the impact force. Aside from the impacts, our models were close to the measured data and were used as a basis for our designs.

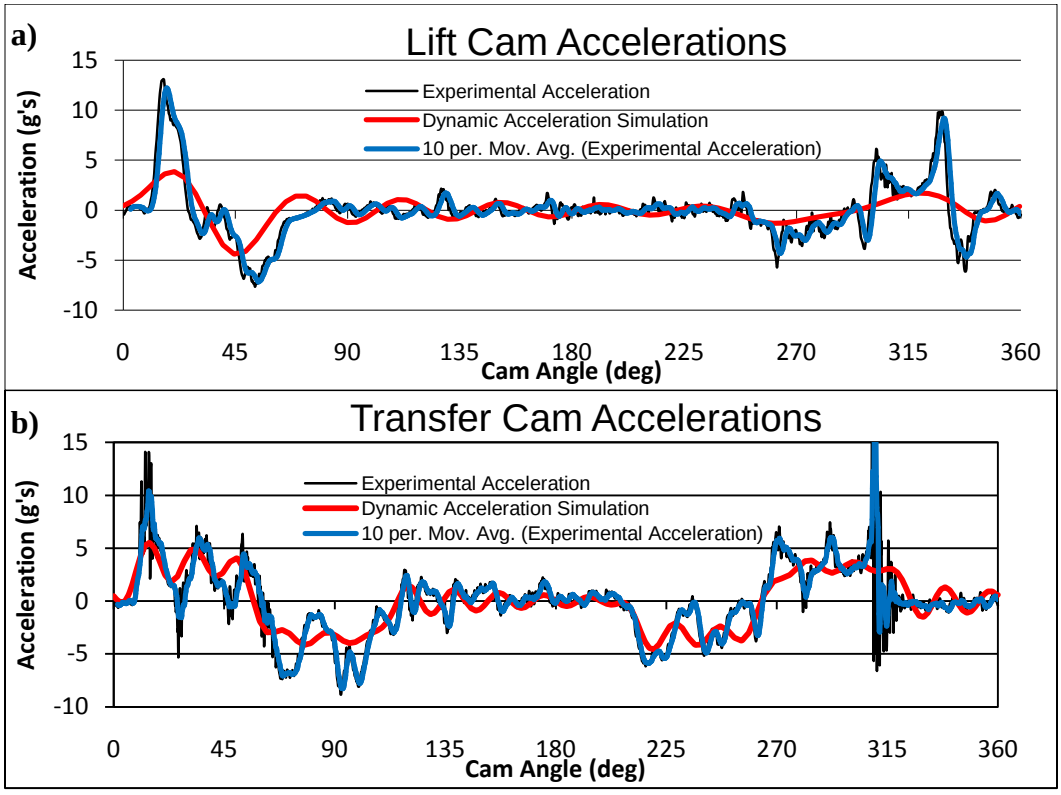

Figure 1: Accelerometer data plotted against our dynamic simulation for the **(a)** Lift Cam **(b)** Transfer Cam

Methods

In order to gently close the nest jaw on Part A, we designed a linear cam with a gently curved spline surface that would ease the nest jaw open prior to placing Part A on the nest. We first needed to calculate the velocity profile of the lift cam end effecter because our linear cam would be attached to it. Our area of focus was on the lift cam rise because that is where the linear cam would be closing the nest jaw, from lift cam angle 233° to 300°. Using the kinematic acceleration from Dynacam and the geometry of the cam train, we calculated the velocity profile of the end effecter. We then designed the surface of the linear cam to have a carefully shaped curve that would ease the jaw closed, based on the calculated velocity profile. We were able to predict the velocity profile of the jaw curving by multiplying the velocity profile of the lift cam velocity by the slope of the linear cam spline curve.

We designed a support for the linear cam that attaches our linear cam to the vacuum pick-up head end effecter. This support acts as a spacer to have the linear cam contact the nest jaw roller with appropriate timing. The support has a locating surface at the top and utilizes the existing screw and dowel holes of the end effecter. Figure 2 shows a side profile of the linear cam and its support mounted to the pick-up head while contacting the nest jaw roller.

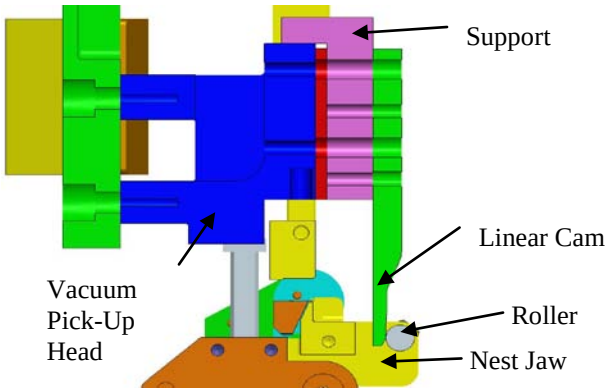

Figure 2: Side Profile of linear cam and support

Transfer Cam redesign

After analyzing the dynamic acceleration of the existing transfer station, we decided to redesign the transfer cam, as a sub-project, to minimize the force at the impact between the end effecter and the hard stop. The current transfer cam profile is defined with modified trapezoidal functions. To better control the acceleration profile, we chose to implement a spline function. We redesigned the cam as a two segment cam.

We tested the redesigned cam using an accelerometer and after examining the results, we discovered an error in our design. Although we did not have time to test a new cam, we did create a second design. This design reverts back to a four segment cam that has a polynomial rise, a dwell, followed by a spline function, used to control the velocity at impact, and finally a second dwell. Because impact force is proportional to velocity, we tried to lower the velocity of the end effecter at impact (311°). Figure 3 shows the velocity profiles of the original and redesigned cams. Our dynamic model predicts that this design will yield a 79% reduction in impact force, while lowering the peak acceleration.

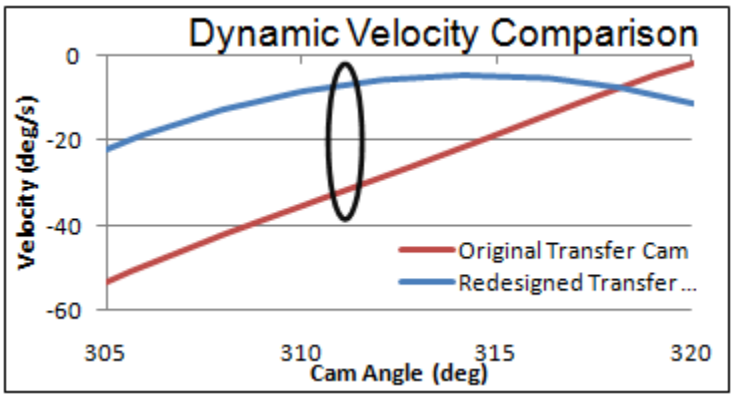

Figure 3: Dynamic velocity of the original and redesigned transfer cam at impact

Conclusions & Recommendations

Our test data show that implementing our linear cam design will gently locate Part A without any product deformation. Testing the linear cam on a manually-driven product assembly machine in a prototype lab proved the basic functionality of the linear cam. On a properly set up station, the cam opened the jaw approximately 0.010 inches and gently closed it.

We also tested the cam on a production machine, which showed the same results when viewed in high-speed video. Using a laser vibrometer to measure the velocity profile of the closing nest jaw, we determined that the data collected during this test matched our predicted velocity, shown in Figure 4, meaning that our design would properly align Part A by gently pushing it in place. Note the spikes before and after the experimental velocity curve. The first spike is due to a slight imperfection at the beginning of the spline curve on the linear cam, while the second one is from the linear cam surface leaving the roller surface just before closing, causing the jaw to snap shut a very small distance. Both of these spikes can be eliminated by replacing the chamfer on our linear cam design with a smooth curve.

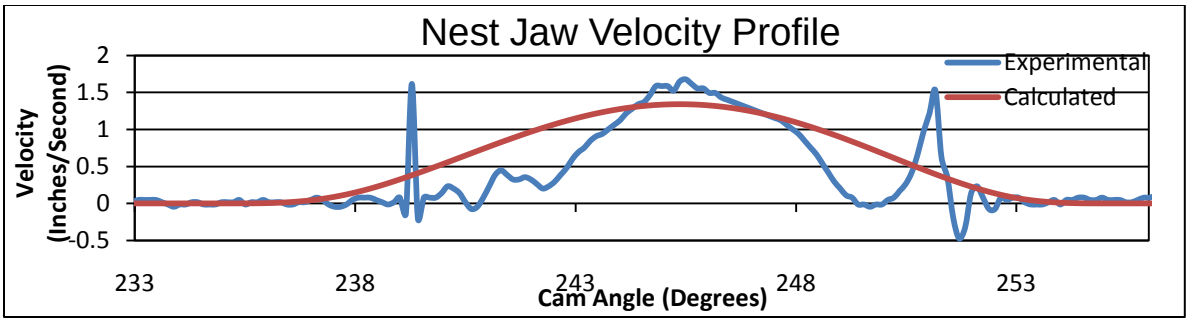

Figure 4: Experimental v. predicted velocities of the nest jaw closing

We predict that our redesigned transfer cam will greatly reduce the velocity at impact. After the results of our accelerometer tests for our first cam redesign were inconclusive, we realized an error in our design and redesigned the cam. Due to time limitations, we were unable to test this design; however, our dynamic simulation suggests a large reduction in impact force.

We recommend that our sponsor conduct further testing of our linear cam. Testing should be performed on a re-made linear cam, on which the chamfer is replaced with a spline curve. In order to fully test the functionality of our design, a more in-depth test should be conducted which completely eliminates the existing registration mechanism and utilizes ours. This test should include regrinding the carbides on the nests 0.003-0.005 inches such that Part A is correctly aligned on the nest. The station set up should be adjusted in order to move the placement of Part A on the nest forward of the closed carbides 0.005 inches. The alignment mechanism in the product fastening station should be disabled when running this test. With this set up, we recommend running production at full speed and determining the impact of our design on product quality.

We also recommend that our sponsor manufacture a prototype of our redesigned cam and repeat our accelerometer testing. After replacing the existing transfer cam with our redesigned cam, the machine should be adjusted according to the existing set up procedures to ensure proper alignment. Accelerometer testing should be conducted on the slice bar to measure the impact force.

Our testing and dynamic simulations show that our linear cam will gently register Part A to a known location, eliminating product deformation. Our final transfer cam redesign suggests that its implementation will reduce the impact force of the end effecter. We hope that our designs and analysis will allow our sponsor to more efficiently produce their product.

Table of Contents

List of Figures

List of Tables

I. Introduction

The high consumer demand for disposable products continuously challenges engineers to devise new, better, and faster methods of production. The assembly of many consumer products is completed on indexing, automatic assembly machines in large factories. Large scale raw materials and pre-fabricated parts are fed into these machines and automatic processes create assemblies, check for quality control and send out the parts to another step in the process. By running many machines at once on the factory floor, manufacturers can easily produce thousands of products per hour, driving down the costs of production.

In order to reinforce this strategy, machines are constantly improved and redesigned to increase production speed and reduce errors. A certain indexing, automatic assembly machine combines Part A and Part B together and outputs the resultant product. The two parts are fastened together, inspected for consistency, and output to another process.

The problem presented to us by our sponsor is that the current alignment method relies on a mechanism pushing on the backside of Part A, pushing the opposite edge into carbide stops to locate it accurately with respect to Part B. The contact forces are sufficient to locally yield the material and cause a small permanent deformation of a few thousandths of an inch. This process is unfavorable for several reasons. The suggested modification was to eliminate this process and move it outside of the fastening box to the Part A placement station, just prior to the fastening station.

II. Background

There are several details that make the current alignment mechanism unreliable. The deformed edge causes problems when feeding into another process and causes high stresses in Part A. Because the stops are attached to a pivoting jaw on the indexing nest, placing Part A on the nest in the previous station with the nest jaw slightly open would allow the stops to push the edge of Part A into alignment by slowly closing the nest jaw. For this process to work on existing machines, the contact points on the stops must be reduced to account for the lack of deformation. This would realign the placement of Part A on the nest so as to place it where the jaw could push against the leading edge when it closes.

The product assembly is currently manufactured on an automated indexing assembly machine. Part A and Part B are fed in from magazines inserted by an operator. By automatic processes, Part B is inserted onto the indexing nest in an earlier station. Part A is then placed on top of Part B and aligned. The two parts are fastened together, inspected for consistency, and output to a magazine for transfer to a subsequent product assembly machine.

In addition to the loading problems in subsequent processes caused by the deformed edge, this process occurs in a sealed off box immediately prior to joining the two parts. This box is difficult to access for repairs and its size greatly limits the capability for modifications to be made.

III. Goal Statement

The goal of our project was to provide our sponsor with a method to accurately locate Part A on top of Part B prior to fastening without locally deforming Part A. We achieved this goal by completing the following objectives:

- Analyze and interpret the existing process to determine what changes are feasible within the process.
- Design a linear cam to gently close the nest jaw, accurately pushing Part A to a known location before fastening to Part B.
- Redesign the transfer cam to reduce the violent impact collision between the slice bar and the hard stop. We added this objective after noticing a very large impact force in our analysis.

The first step of this improvement was to analyze the existing placement station. This required a 3D CAD model created from detail drawings that simulates the layout of the machine and the physical motions of the linkages and sliders. From this we created kinematic and dynamic models of the motions using the CAD model and Dynacam software. With this data, we compared our calculated accelerations to data collected using accelerometers on existing machines in the factory. After analysis of these data, we made adjustments to our kinematic and dynamic models to improve the correlation between calculated and experimental data. We also discovered large impact forces due to the design of the transfer cam in the station.

After this analysis, we outlined our two main changes. We planned to reduce the impact forces by redesigning the transfer cam with a more efficient cam design strategy. By reducing the velocities at impact, we could reduce impact forces and reduce high accelerations from rapid stops. Second, we designed a linear cam to create a controlled opening and closing motion on the pivoting jaw of the indexing nest. We used Dynacam to create a cam surface that would control the velocity of the jaw so as to prevent violent impacts between the stops and Part A and reduce vibrations in the pivoting jaw. This would ensure accurate alignment of Part A to Part B and prevent crush damage and reduce stresses in Part A.

IV. Analysis

Before attempting to redesign any part of the product assembly machine, we analyzed the existing conditions of the transfer station, station 5. We created an overall assembly of the transfer station in ProEngineer to verify the motions of our model and check for interference. By modeling the existing cams using Dynacam software, Cam Design Software, written by Professor Robert L. Norton, P.E., we were able to create several models and simulations, which we later used to compare to data measured on the machine with accelerometers. We simplified the cam trains to equivalent mass-spring models so the dynamics could be simulated within Dynacam. These simulations served as a basis of comparison against our accelerometer data both to check the accuracy of our model and to use as a starting point for designing a new model.

The transfer station receives Part A from a feed magazine and places them on the nest aligned in two directions for later assembly. The final alignment is done in the attachment box as described before. The placement of Part A is done using two separate cam-follower trains. The transfer cam is the horizontal motion and the lift cam is the vertical motion. The transfer cam system has a lower lever arm, a connecting rod, an upper lever arm, and the final slice bar end piece. The connecting rod length, the lever arm length and the position of the slice bar slide can be adjusted to set up the machine. The lever arm and connecting rod can also be adjusted on the lift cam train for adjustment.

The transfer cam slider moves a slice bar to push Part A from the bottom of the magazine to the vertical pick-up head as shown in Figure 5 (a). The vertical pick-up head is attached to the Lift Cam. In Figure 5 (b), both cams are dwelling and the vacuum on the pick-up head picks up Part A. In Figure 5 (c), the slice bar returns to pick-up another Part A while the pick-up head lowers to place the part on the nest and in Figure 5 (d), the pick-up head is dwelling as the vacuum turns off and the magnets on the nest secure the position of Part A on the support. In Figure 5 (e) and Figure 5 (f), the transfer cam dwells as the pick-up head travels up again and then the lift cam dwells as another part is pushed under the pick-up head.

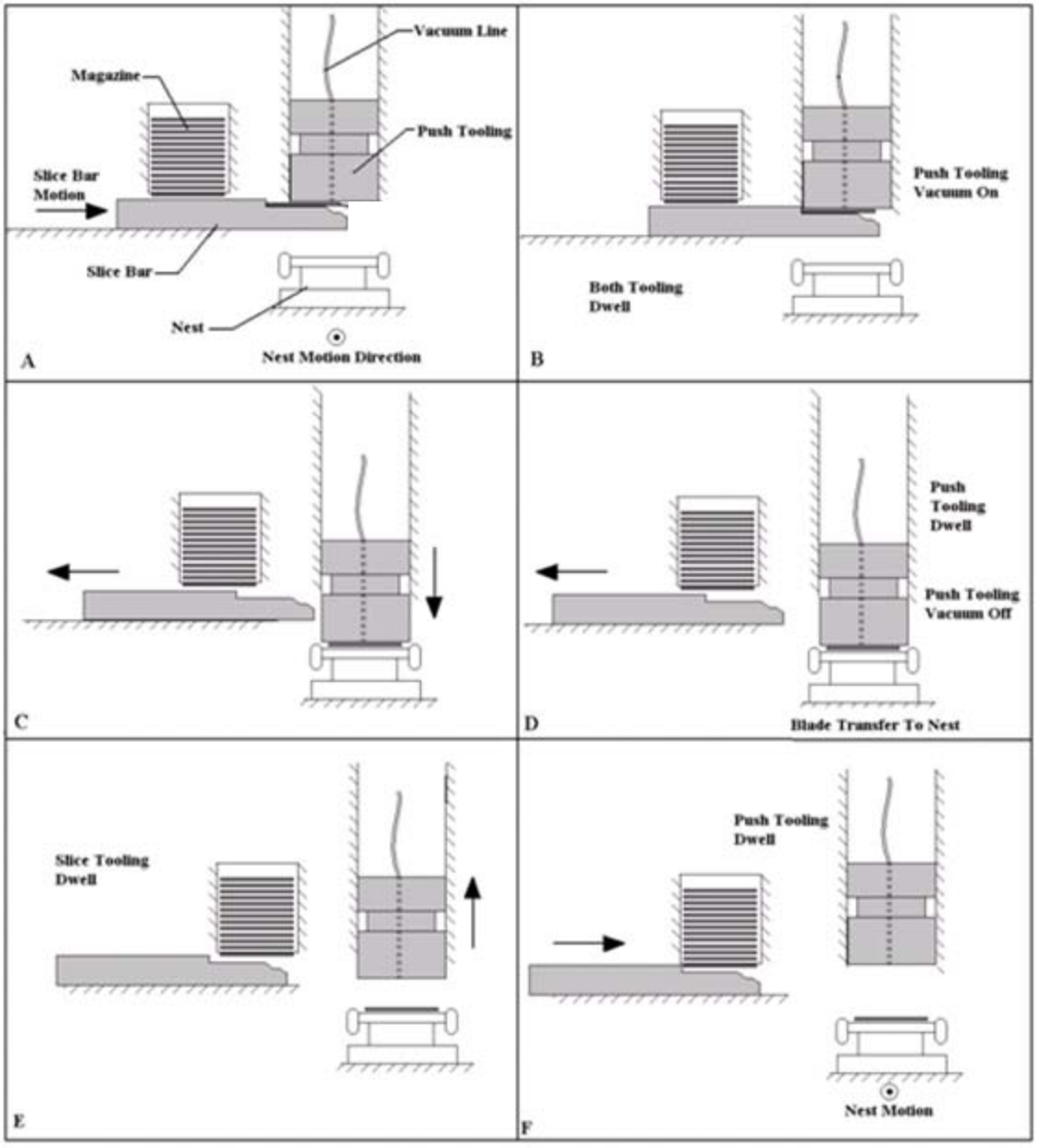

Figure 5: Product pick-up and placement

System Model Using CAD Software

To accurately model the physical movements of the end effecters, we modeled all the components of the transfer station in ProEngineer. After building each part individually, we built sub-assemblies, and eventually an overall model of each cam train. This model allows us to accurately study the interactions between the two end effecters. Figure 6 (a) shows the overall assembly of the transfer station, including both cam trains in their entirety and the chassis of the product assembly machine. Figure 6 (b) shows a close-up of the end effecters. Note the very small (approximately 0.25 mm) gap between the slice bar and the vacuum head. Because these two parts interact very close to one another, we wanted to ensure that our design would not result in any interference between these two parts.

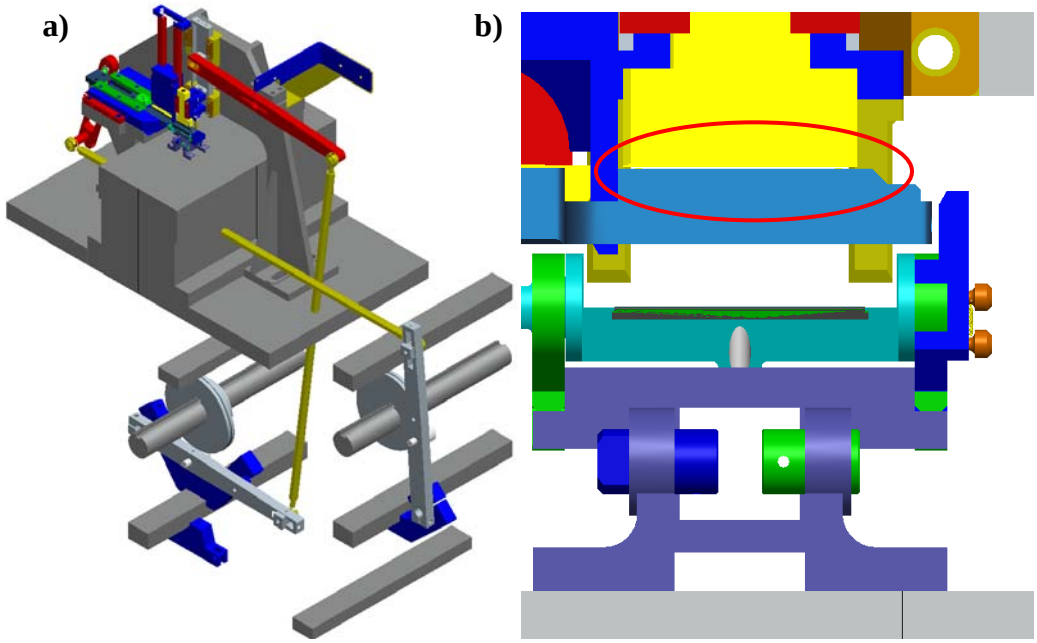

Figure 6: (a) Overall model of both cam trains **(b)** Close-up of both end effecters

Using the Mechanism Program within ProEngineer, we added applicable constraints such that our model could most accurately mimic the movements of the transfer station. Figure 7 shows all of the constraints added to the overall assembly. The blue arrows represent the forces of the air cylinder springs holding the cam lever arm against the cam. The cam outlines are highlighted in light blue to show that they have a cam surface connection to the rollers, meaning that the surfaces must always be tangent. All pin and slider rotations are also defined. To drive

the system, a “servo motor” is added to each cam. Both cams move at the same speed in the model as they actually do on the machine.

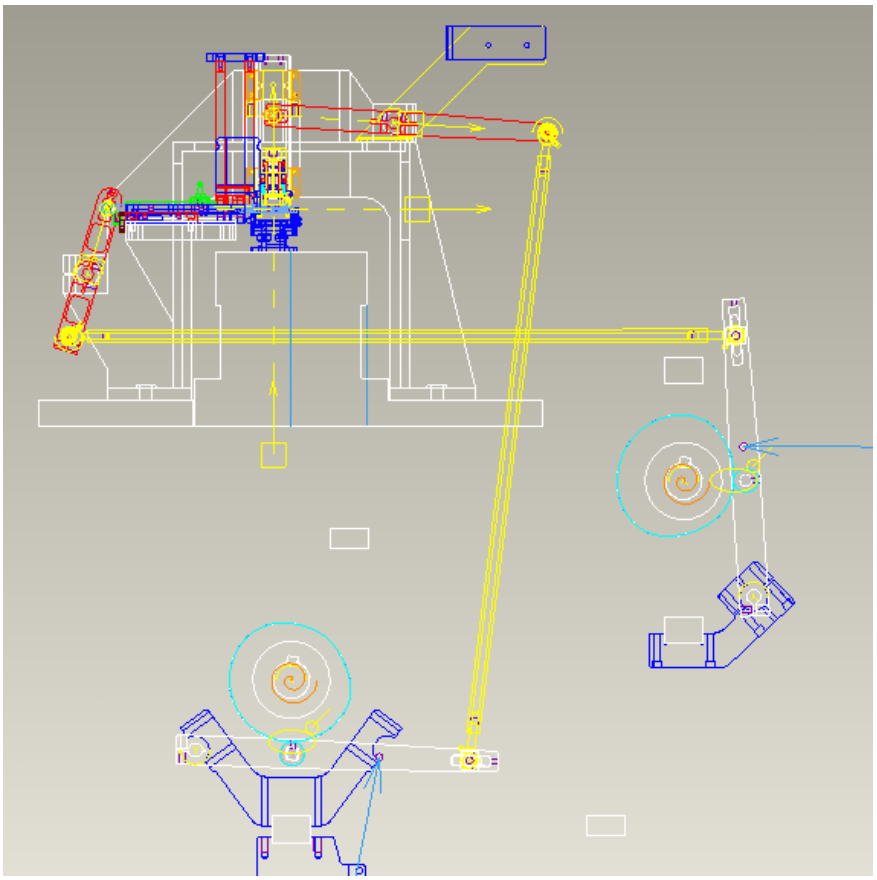

Figure 7: Overall assembly of the transfer station with dynamic constraints

Effective Mass Models

The motions of the transfer station are controlled by two cams, one that moves a vertical slider (lift cam), and another that slides a horizontal slice bar (transfer cam). Both of these cam trains can be treated like a series of springs and masses, all cam-driven. We modeled each cam train as a one degree of freedom (DOF) model in Dynacam. The end effecter of the lift cam is effectively a second DOF; however, we could not place an accelerometer on the vacuum pick-up head, so our accelerometer was placed on the vertical slider, which is equivalent to the end effecter of a one DOF model.

Figure 8 and Figure 9 show both cam trains of the transfer station. The two cam trains have different functions and are in different orientations; however, it can be seen that the two

cam trains are comprised of the same basic components. Because of the similar structures of the cam train, we were able to use the same model for both cam trains, with different values.

While modeling the parts in Pro Engineer, we paid close attention to planar references, so any information regarding the geometry of the part could be easily obtained later on. After applying proper material properties, we were able to gather all necessary data to create a simplified dynamic model, including part lengths, material moduli of elasticity, cross-sectional areas, masses, and moments of inertia. Using this information, we were able to simplify each cam train to an equivalent system with one equivalent mass and one equivalent spring constant.

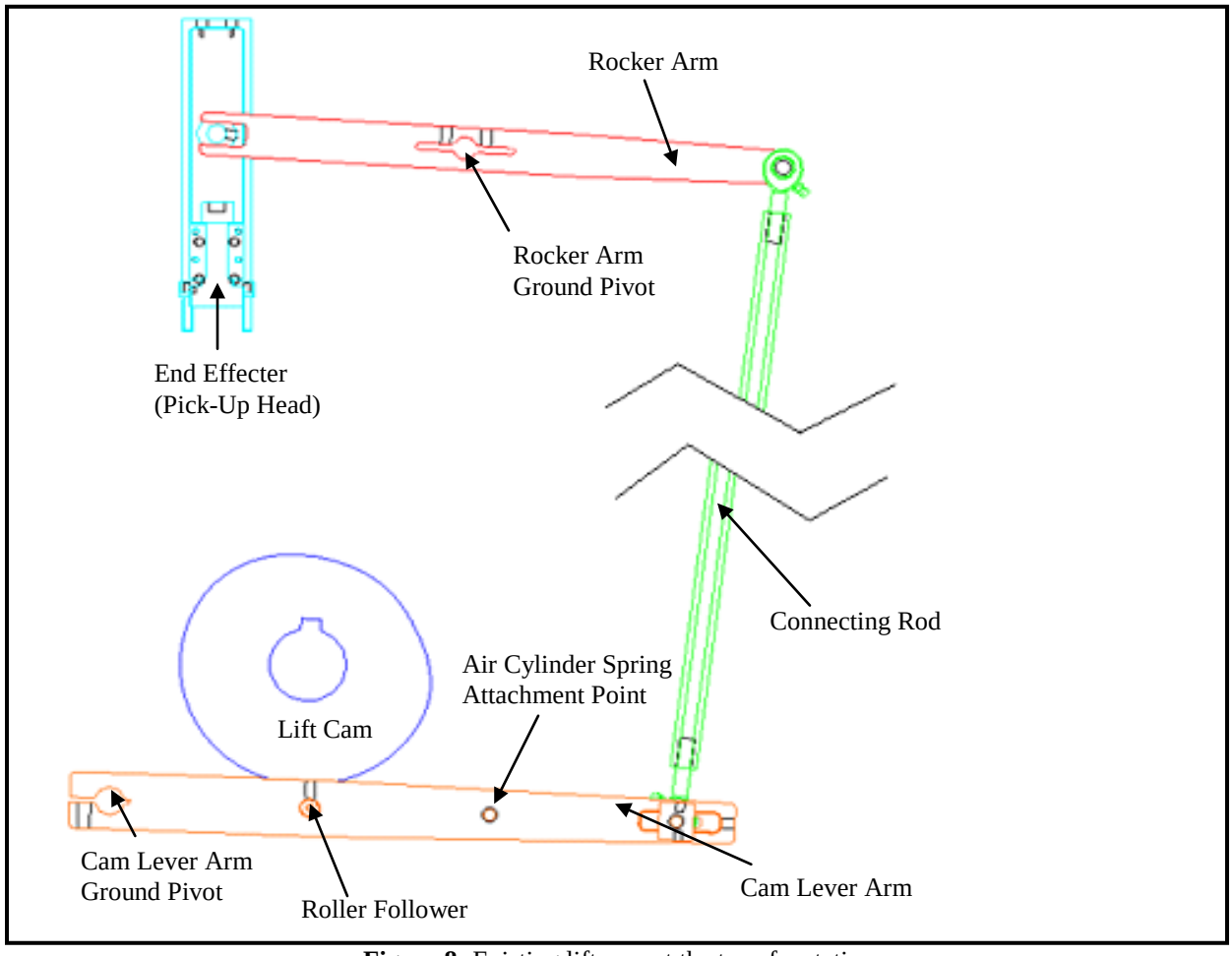

Figure 8: Existing lift cam at the transfer station

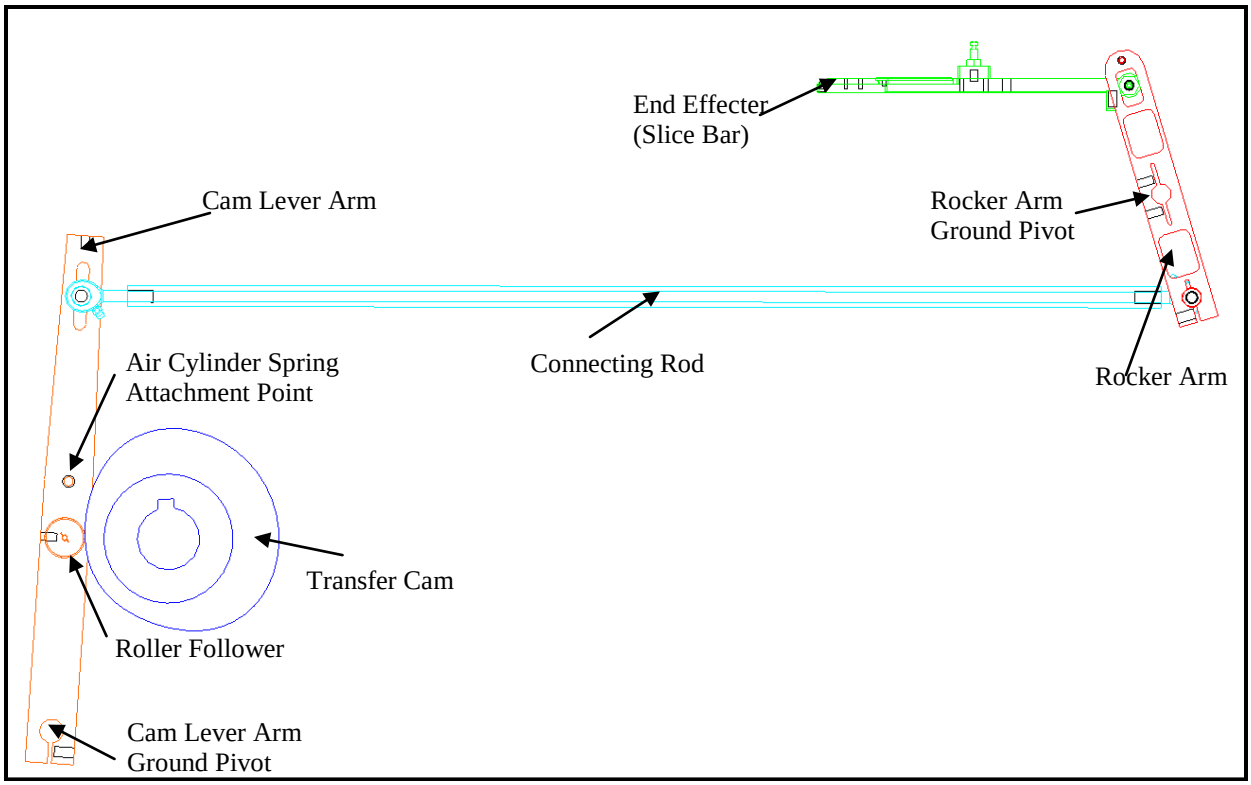

Figure 9: Existing transfer cam at the transfer station

Each member of the cam train can be modeled as a point mass with an equivalent spring constant, k. Figure 10 (a) shows the lift cam train modeled in this manner and Figure 10 (b) shows an overall model with an effective mass (m_{eff}) and effective spring constant (k_{eff}). The masses of each component were determined in ProEngineer. The spring constants were determined by either static analysis or finite element analysis (FEA) of the parts deflection under load. By using the geometry of the system, the individual masses and spring constants can be accurately combined as one effective mass and one effective spring constant. This section details the calculations for the lift cam train; the same procedure was used for the transfer cam train as well.

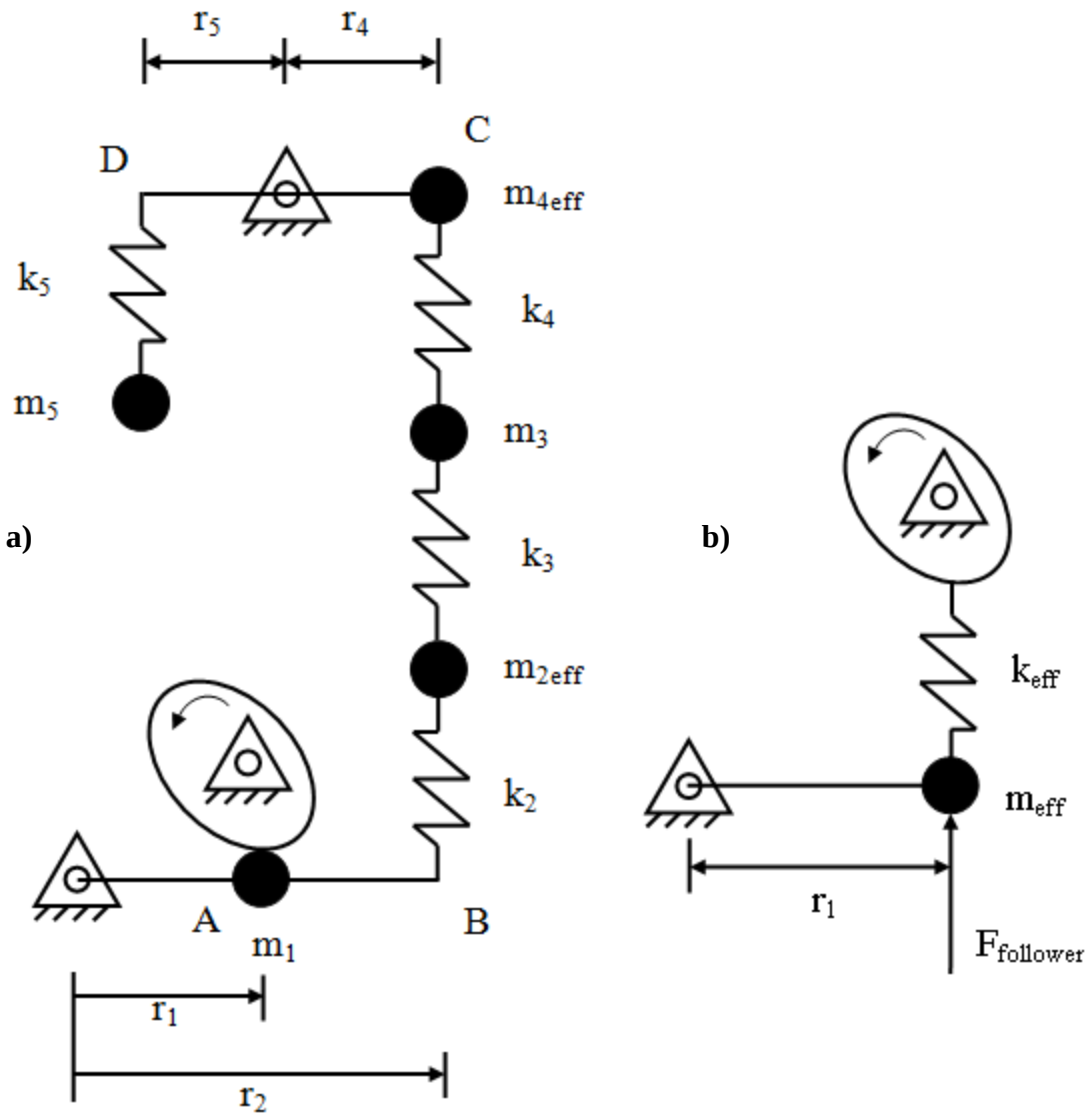

Figure 10: (a) Overall cam train lumped mass model **(b)** Equivalent system model

In order to determine the effective masses of the system, we first needed the masses of each individual component. In Figure 10, the mass of the roller is represented by m_1 and the mass of the connecting rod is represented by m_3. These are the only known mass values. We determined m_5 by adding the masses of all components moving together with the end effecter, treating them as a "lumped" mass. The masses of the rocker and cam lever arm are not explicitly used; however, their effective masses are needed (m_{4eff} and m_{2eff}, respectively). The effective mass of these components represents point masses with respect to the pivot axis. Using the definition for moment of inertia, $dI = r^2 dm$, we calculated the effective masses, treating each

link as a long, slender member, listed as equations (1) and (2). I_{zz4} and I_{zz2} are the moments of inertia of the rocker arm and the cam lever arm, respectively, about their axes of rotation.

$$m_{4eff} = \frac{I_{zz4}}{r_4^2} \quad (1)$$

$$m_{2eff} = \frac{I_{zz2}}{r_2^2} \quad (2)$$

Once m_1, m_{2eff}, m_3, m_{4eff}, and m_5 were determined, we simply "moved" the masses to point A. The effective mass of m_5 at point C is calculated my multiplying by the square of the lever ratio.

$$m_{5C} = m_5 \left(\frac{r_5}{r_4}\right)^2 \quad (3)$$

The total mass at point C is then calculated and is simply the sum of the effective mass of the rocker arm and m_5 at point C.

$$m_C = m_{5C} + m_{4eff} \quad (4)$$

Because m_C, m_3, and m_{2eff} all lie along the same line, the mass at point B is simply the sum of these three masses.

$$m_B = m_C + m_3 + m_{2eff} \quad (5)$$

Finally, the overall effective mass for the system is determined by "moving" the mass at point B to point A and adding the mass of the roller, m_1.

$$m_{eff} = m_B \left(\frac{r_2}{r_1}\right)^2 + m_1 \quad (6)$$

The next component of the model is an overall effective spring constant, which is obtained in a similar manner. We conducted FEA on several components in order to determine their individual spring constants. The spring constant of the cam follower arm is represented by k_2. Because the rocker arm pivots around a ground point, it is treated as two springs with

constants k_4 (connecting rod side) and k_5 (end effecter side). Note that this model does not include k_1. This is because k_1 represents the air cylinder spring, which applies resistance in the opposite direction as this spring system.

The lever arm and cam follower arm were imported into SolidWorks software from ProEngineer to do this. Appropriate boundary conditions were applied to mimic the loading situation that each component endured on the machine. We applied arbitrary loads of 400 Newtons to measure the deflection with a known force. Once proper restraints and loads were applied, SolidWorks simulated the actual deformation of the parts, which cannot be accurately calculated by hand due to irregular geometry. We then used Hooke's law, $F = kx$, to determine the spring constant. Figure 11 shows the cam follower arm (for the lift cam) with the pivot and roller restrained and a force applied to the point that attaches to the connecting rod. The spring constant is then calculated by simply dividing the known force (400N) by the displacement at the joint. This method is used to calculate k_2, k_4, and k_5.

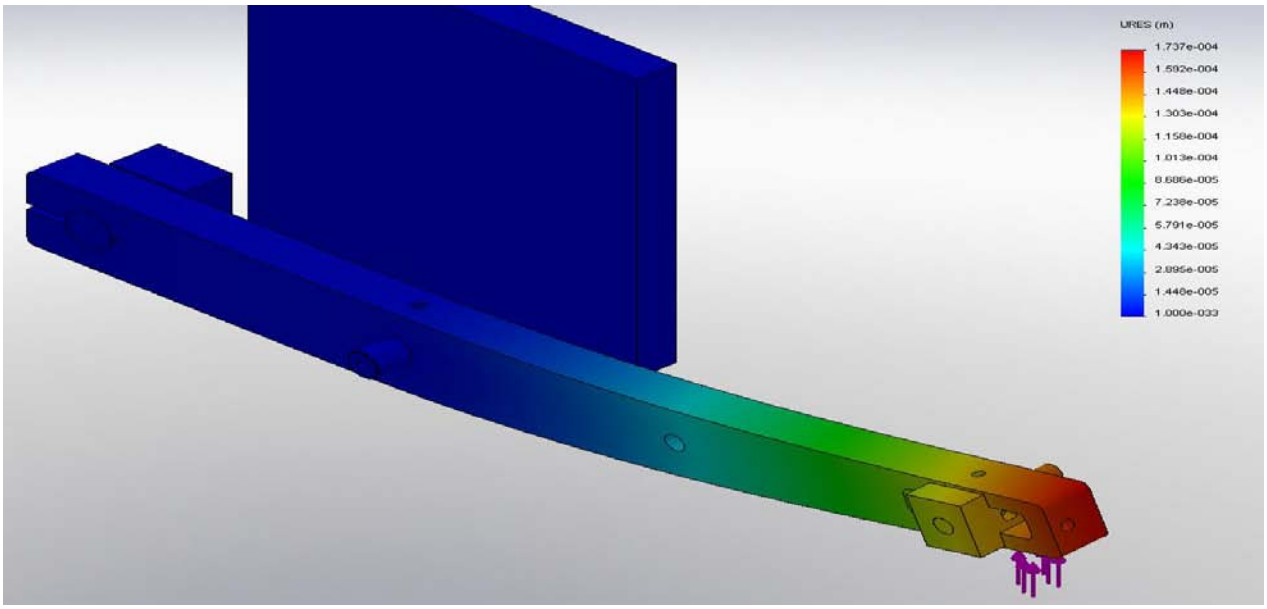

Figure 11: Example of FEA analysis, showing the lift cam follower arm subjected to 400 N

Using ProEngineer to obtain the cross-sectional area (A), modulus of elasticity (E), and pin-to-pin length (L), we found the spring constant of the connecting rod, k_3.

$$k_3 = \frac{AE}{L} \tag{7}$$

Once k_2, k_3, k_4, and k_5 are known, we can determine an overall effective spring constant. The first calculation in this series is to move k_5 across the rocker arm to point C.

$$k_{5C} = k_5 \left(\frac{r_5}{r_4}\right)^2 \tag{8}$$

The effective spring constant at point B simply adds the spring constants of spring 5 at point C, spring 4, spring3, and spring 2 in series.

$$k_B = \frac{1}{\frac{1}{k_2}+\frac{1}{k_3}+\frac{1}{k_4}+\frac{1}{k_{5C}}} \tag{9}$$

Finally, we "moved" the spring constant at point B to point A, using the same ratio as used in the mass calculation.

$$k_{eff} = k_B \left(\frac{r_2}{r_1}\right)^2 \tag{10}$$

All calculations were executed using Microsoft Excel and are included in Appendix A. The same procedures to calculate k_{eff} and m_{eff} were used to model the transfer cam train. The values used and final values obtained are shown in Table 1 and Table 2.

Table 1 – Input variables, effective masses, and effective spring constant for the lift cam train

Lift Cam					
Constants Used	Component	Mass, kg	Component	FEA Δx, mm	k, N/m
$A=1.76x10^{-4}$ m^2 E=68.9 GPa L=0.762 m $I_{zz4}=0.013$ kg-m^2 $I_{zz2}=0.085$ kg-m^2	End Effecter	$m_5=0.833$	Rocker (EE side)	0.12	k_5=3,433,000
	Rocker	$m_{4eff}=0.336$	Rocker (CR side)	0.23	k_4=1,728,000
	Connecting Rod	$m_3=0.473$	Connecting Rod	--	k_3=15,967,000
	Cam Lever Arm	$m_{2eff}=0.655$	Cam Lever Arm	0.15	k_2=2,697,000
	Roller Follower	$m_1=0.136$	--	--	--
Effective Value		$m_{eff}=14.63$			k_{eff}=654,276

Table 2 – Input variables, effective masses, and effective spring constant for the transfer cam train

Transfer Cam					
Constants Used	Component	Mass, kg	Component	FEA Δx, mm	k, N/m
$A=1.77x10^{-4}$ m^2 E=68.9 GPa L=0.813 m $I_{zz4}=0.002$ kg-m^2 $I_{zz2}=0.082$ kg-m^2	End Effecter	$m_5=0.473$	Rocker (EE side)	0.24	$k_5=1,660,000$
	Rocker	$m_{4eff}=0.294$	Rocker (CR side)	0.12	$k_4=3,258,000$
	Connecting Rod	$m_3=0.493$	Connecting Rod	--	$k_3=15,001,000$
	Cam Lever Arm	$m_{2eff}=0.700$	Cam Lever Arm	0.081	$k_2=4,914,000$
	Roller Follower	$m_1=0.136$	--	--	--
Effective Value		$m_{eff}=11.65$			$k_{eff}=1,065,000$

To more accurately model the *entire* system, the air cylinder spring and damping coefficients of the system must be taken into account. The air cylinder spring constants and spring preloads were determined using the initial pressure of the cylinder, P_0, with respect to atmospheric pressure (P_{atm}), as well as the geometric properties of cross-sectional area (A_C), volume (V_0), and stroke length (x). Note that the spring constant, k_a, is the derivative of the spring preload, F_0, with respect to x. Table 3 shows the spring constants of the air cylinder springs attached to the cam lever arms, their corresponding preloads, as well as the given and measured variables used in their calculation.

$$k_a = \frac{A_C^2 V_0 (P_0 + P_{atm})}{(A_c x - V_0)^2} \tag{11}$$

$$F_0 = \frac{A_C V_0 (P_0 + P_{atm})}{(A_c x - V_0)} - P_{atm} A_C \tag{12}$$

Table 3 – Input variables, effective spring constants, and spring preloads for the air cylinder spring

Variable	Lift Cam	Transfer Cam
Cross-Sectional Area (A_c)	6.143x10-4 m^2	6.143x10-4 m^2
Volume (V_0)	3.258x10-5 m^3	1.629x10-5 m^3
Initial Pressure (P_0)	552 kPa	552 kPa
Atmospheric Pressure (P_{atm})	101 kPa	101 kPa
Stroke Length (x)	0.216 m	0.009 m
Air Cylinder Spring Constant (k_a)	25,018 N/m	41,143 N/m
Spring Preload (F_0)	665 N	597 N

Figure 12 represents a full dynamic model of the cam system, where the cam is pushing on an infinitely rigid, mass-less plate, which in turn moves the effective calculated above. The air cylinder spring and a damper, c_1, act between the cam and the plate; while the effective spring constant and a damper, c_2, act between the infinitely rigid plate and the effective mass. The

distance *s* is the kinematic motion of the cam and the distance *x* is the dynamic motion of the end effecter, as mathematically predicted. The damping coefficients, c_1 and c_2, are calculated internally within Dynacam given two assumed damping ratios, ζ_1 and ζ_2, using $c = 2\zeta\sqrt{km}$. The damping ratios are defined based on experimental data from similar machines.

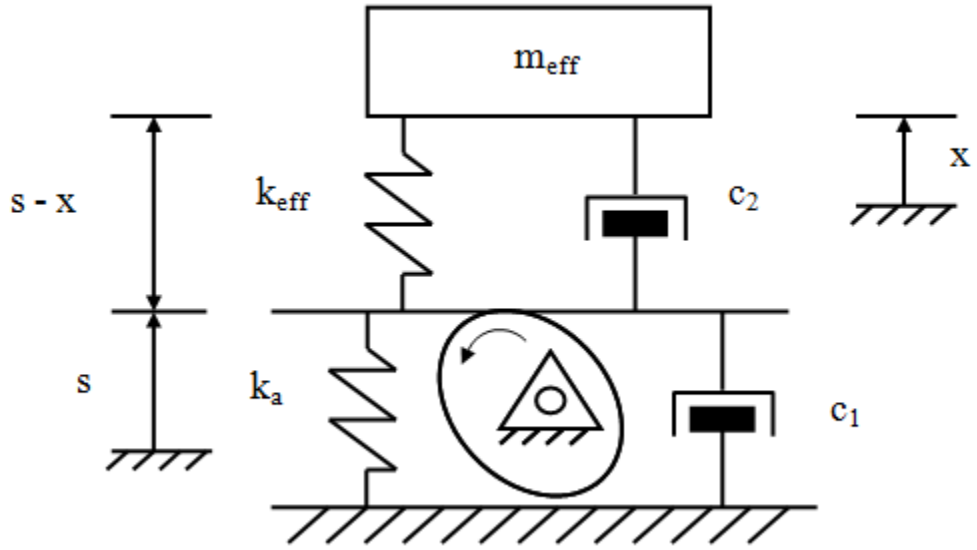

Figure 12: Dynamic model of the cam driving the effective mass of the system

Modeling the Existing Cams

In order to simulate the dynamic motions of the end effecters, we first used the constants calculated in "Effective Mass Models" to recreate the existing cams using Dynacam software. Once these cams were recreated, we were able to use them not only for predicting dynamics, but also to recreate the dynamic motions of both end effecters in ProEngineer by exporting the cam profiles.

Transfer Cam

As with any cam design, we began by defining the inputs at the SVAJ (displacement, velocity, acceleration, jerk) screen. The transfer cam is a four-segment, double-dwell cam that consists of a rise, a dwell (a cam segment with a constant radius and therefore no motion), a fall, and a second dwell. Both the rise and the fall are modified trapezoid functions, named so

because the acceleration function resembles a trapezoid with rounded edges. The cam begins its motion 45° relative to machine zero, so we defined cam zero to be 45° and the rotation speed was set to machine speed. Table 4 shows the values used at the Dynacam SVAJ screen, where β is the angular duration of each segment with respect to the camshaft. The initial and final positions are given in degrees of rotation of the follower arm.

Table 4 -- Dynacam SVAJ screen input values for the transfer cam

β	Start	End	Motion	Program	Initial Position	Final Position
115°	0°	115°	Rise	Modified Trapezoid	0°	8.143°
90°	115°	205°	Dwell	Dwell	8.143°	8.143°
120°	205°	325°	Fall	Modified Trapezoid	8.143°	0°
35°	325°	360°	Dwell	Dwell	0°	0°

After defining the motions of the cam, we drew a cam profile by defining the prime radius, the roller radius, and the cutter radius, which are 81.25 mm, 15.88 mm, and 203.2 mm, respectively. The follower arm radius was defined as 152.4 mm, rotating about the point (x,y) = (92.07 mm, -151.41 mm) with respect to the center of the camshaft. The cam profile is calculated internally within Dynacam, along with the pressure angles and radii of curvature. When designing cams, we would try to keep the pressure angle below 30° and the radius of curvature should be twice that of the follower radius. Although we cannot change these values, we verified that they both fell into the appropriate ranges.

We created the dynamic simulation of the end effecter by inserting the values calculated in "Effective Mass Model" in the *Dynamics* and *Vibration* screens in Dynacam, where m=meff, $k_1=k_a$, $k_2=k_{eff}$, and ζ_1 and ζ_2 are assumed to be 0.05. The Dynacam simulation predicts the vibrations of the end effecter and superimposes them upon the theoretical kinematic motions.

Figure 13 shows the simulation results plotted on top of the theoretical kinematic acceleration. The superposition of the kinematic acceleration and vibration analysis is apparent in that the "base curve" of the dynamic simulation is the kinematic acceleration. It can be seen that where the kinematic trapezoidal acceleration "levels off", the end effecter continues to accelerate. The peak dynamic acceleration is nearly twice that of the kinematic acceleration, which is important to consider when minimizing accelerations. Furthermore, during the dwell periods, the kinematic acceleration is zero; however, the dynamic simulation shows that the end effecter continues to vibrate in spite of the cam rotating at a constant radius. We later verified

this shape against the actual motions of the end effecter, measured with an accelerometer. This model was then used to predict the motions of our new cam designs.

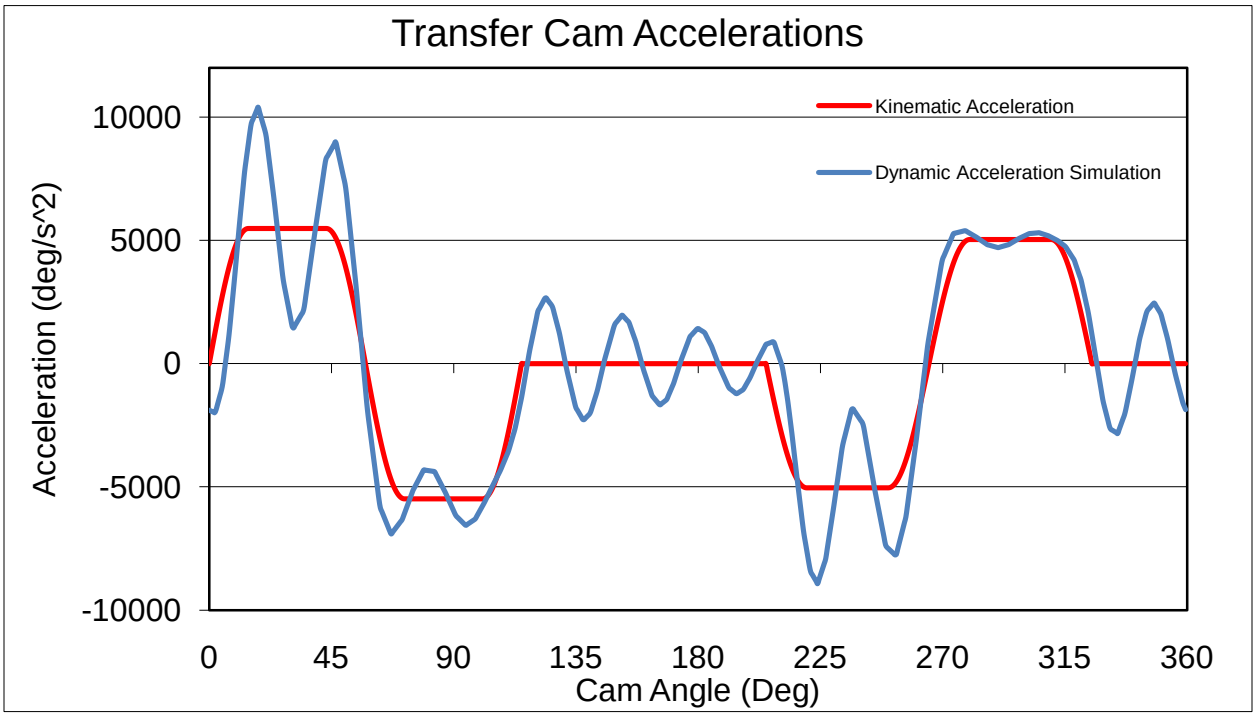

Figure 13: Theoretical kinematic acceleration and dynamic acceleration simulation for the transfer cam

Lift Cam

The process for recreating the lift cam was similar to that of the transfer cam with a few additional steps. The lift cam is also a four-segment, double-dwell cam; however, rather than modified trapezoidal functions, the lift cam utilizes polynomial functions during the rise and fall motions. Table 5 shows the inputs to the SVAJ screen, where the positions are again given as the degrees of rotation of the follower arm.

Table 5 – Dynacam SVAJ screen input values for the lift cam

β	Start	End	Motion	Program	Initial Position	Final Position
67°	0°	67°	Polynomial	Poly	0°	4.2069°
170°	67°	237°	Dwell	Dwell	4.2069°	4.2069°
97°	237°	334°	Polynomial	Poly	4.2069°	0°
26°	334°	360°	Dwell	Dwell	0°	0°

The motion of a modified trapezoidal function is calculated internally within Dynacam; however, a polynomial function requires boundary conditions to be given. The displacement function for a polynomial follows the form shown below, where n is the *degree* of the polynomial.

$$s = C_0 + C_1 x + C_2 x^2 + \cdots + C_n x^n \qquad (13)$$

The number of boundary conditions required is equal to the *order* of the polynomial, which is one more than the polynomial degree. The lift cam is a sixth degree (seventh order) polynomial, requiring seven boundary conditions. The displacements at the end points are two of the conditions. The other five boundary conditions control the velocity and acceleration at the end points or at a known point. Table 6 gives the boundary conditions used to recreate the cam for both the rise polynomial and the fall polynomial.

Table 6 – Dynacam boundary conditions for the polynomial rise and fall functions for the lift cam

Rise				**Fall**			
θ	**0°**	**30°**	**67°**	**θ**	**0°**	**55°**	**97°**
s	0	--	4.2069	s	4.2069	--	0
v	0	--	0	v	0	--	0
a	0	0	0	a	0	0	0
j	--	--	--	j	--	--	--

After defining the cam motions, we drew the cam profile, following the same procedures as for the transfer cam. The prime radius, roller radius, and cutter radius were defined as 87.7 mm, 15.9 mm, and 203.2 mm, respectively. The follower arm was defined as having a radius of 127 mm at a location (x,y) = (-125.7 mm, -92.1 mm) with respect to the center of the camshaft.

The values input to the "Dynamics" and "Vibration" screens in Dynacam were again the effective values calculated in "Effective Mass Model" and the damping ratios, ζ_1 and ζ_2, were assumed to be 0.05 again. Figure 14 shows the dynamic simulation of the end effecter acceleration and the kinematic acceleration of the follower, plotted on the same axes. Like the transfer cam, the lift cam also continues to accelerate beyond the peak kinematic acceleration, according to the dynamic prediction. During the long dwell after the rise, the dynamic simulation continues to oscillate; however, it can be seen that there is an exponential decay in amplitude, controlled by a decreasing "envelope" over the dwell. It should be noted that because

the second dwell is considerably shorter, the oscillations do not have as much time to decay before entering the rise again.

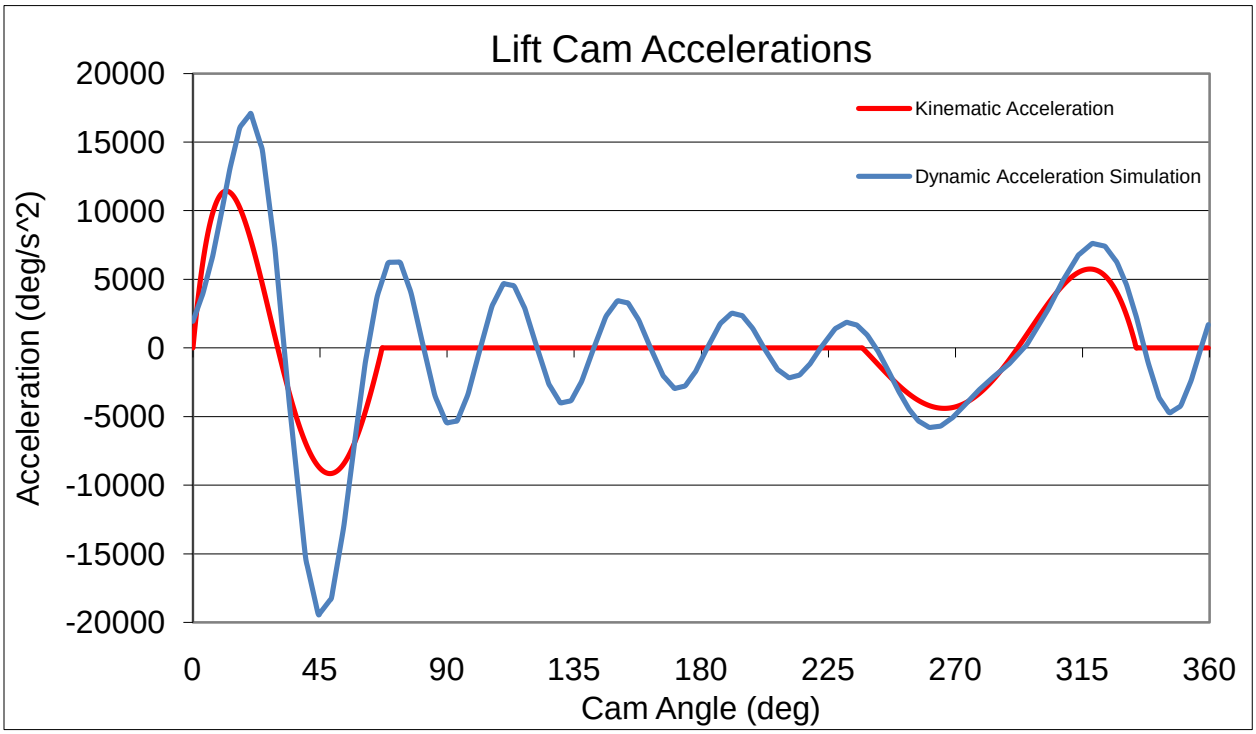

Figure 14: Theoretical kinematic acceleration and dynamic acceleration simulation for the lift cam

Analyzing the Existing System Accelerations

We used accelerometers to measure the acceleration of each end effecter on a production machine at the sponsor company. This data shows us how accurate our models are, but also provides some information that cannot be theoretically predicted. Figure 15 shows our experimentally measured data plotted on the same axes as the acceleration simulation calculated in Dynacam. To clarify the experimental data, a moving average was plotted over it, to smooth the line, making it easier to compare. The experimental data has a large amount of electrical and mechanical noise, shown as rapid vibrations throughout the entire data series. The moving average smoothes this, but it cannot be eliminated because there is a great deal of impacts throughout the entire machine, which travel to the accelerometer.

Our acceleration was measured in g's (the acceleration due to gravity is equal to one "g"), but our dynamic acceleration simulation was output in deg/s^2, which is the angular acceleration of the cam lever arm, not the linear acceleration of the end effecter. To convert from angular

acceleration (in deg/s^2) to linear acceleration (in g's), we used a simple ratio. Although this is not an exact conversion, it is a very close linear approximation.

It can be seen that the frequency of the measured data is slightly higher than that of the dynamic simulation, suggesting that there could be a slight inaccuracy in our calculated spring constant. This is likely due to the FEA process, which estimates the spring constant based on a linear, ideal spring. During the cam rise, the acceleration is much larger than predicted in Dynacam. The beginning of the dwell (67°) can be seen as a rapid change in slope of the moving average (and experimental data). During the cam fall, the vacuum is being lowered towards the nest and two shot pins are inserted into slots in the nest to lock its location. This is the cause of the two larger spikes at the end of the fall. We verified this by observing the data being taken simultaneously with a high speed camera showing the movement of the end effecter.

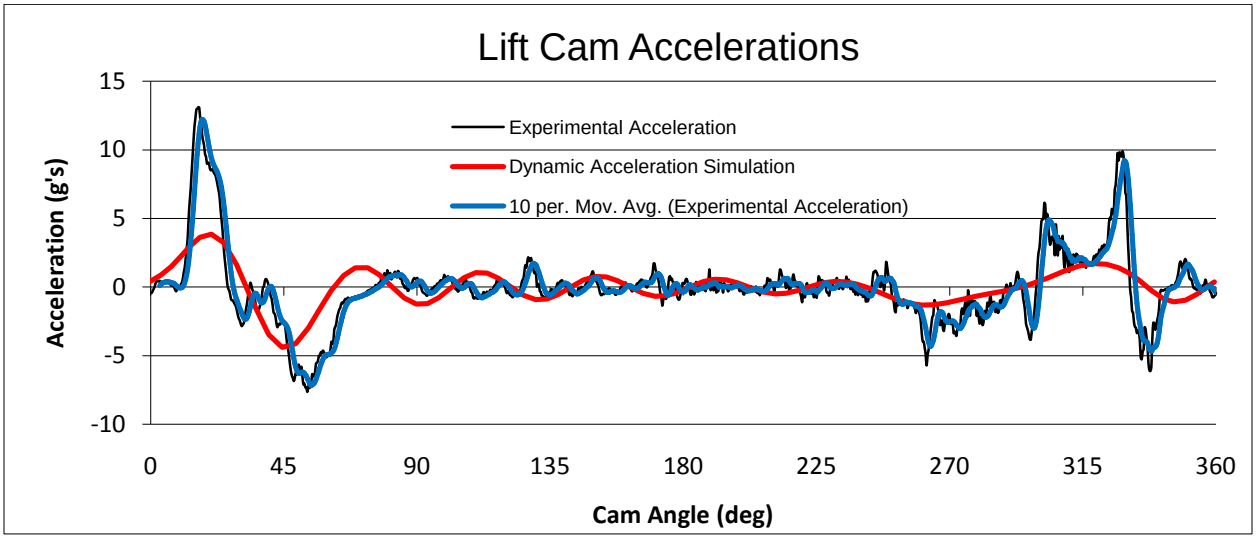

Figure 15: Experimentally measured lift cam accelerations plotted against the dynamic acceleration simulation

We followed the same procedures for the transfer cam acceleration data. Figure 10 shows the transfer cam acceleration profile. One unexpected result that we noticed was a very large spike in acceleration, peaking at nearly 48 g's or 80,000 deg/s^2. This spike is shown in its entirety in Figure 16 (a). Figure 16 (b) shows the acceleration data with the spike truncated at 15 g's, so the acceleration profile can be more clearly seen. After watching the motions with a high speed camera, it was determined that this spike was caused by an impact between the end effecter and a hard stop. Through Newton's Second Law, $F = ma$, force is proportional to acceleration, meaning that a large spike in acceleration will lead to a large force. A repeating

impact force can lead to fatigue failures over time, so we saw an opportunity to improve this cam train. By designing the cam to have a lower velocity, we can reduce the impact force because impact force is directly proportional to velocity.

$$F_i = v\sqrt{\eta k m} \tag{14}$$

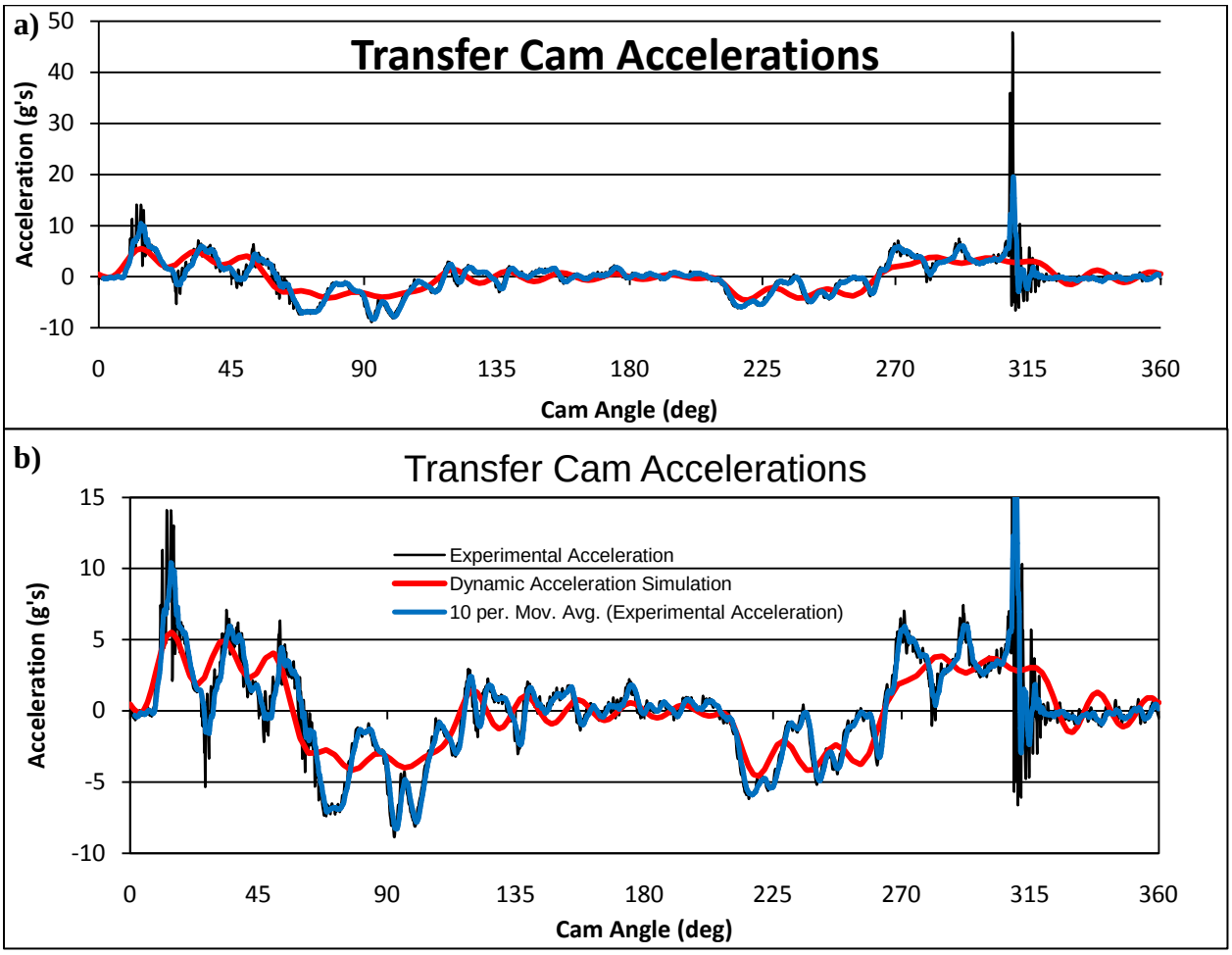

Figure 16: (a) Transfer cam accelerations shown in full **(b)** Transfer cam accelerations with the spike truncated

V. Methodology

The goal of this project was to utilize the existing tooling and their motions to control the alignment of Part A to Part B. The purpose of the linear cam was to use the vertical motion of the lift cam mechanism to orient Part A. The linear cam is directly attached to the pick-up head or the end effecter of the lift cam mechanism. Therefore, the motion of the linear cam is constrained by the mechanism's existing motion. This linear cam was designed to replace the current positioning function, creating a less traumatic way to align the product on the nest before welding. The idea was to use the carbide stops on the jaw to move Part A into the correct orientation rather than forcing Part A into the stops, which is the current method used. The goals were to use this cam surface to control the distance the jaw opened and the velocity at which the jaw closed. The jaw's rotational speed had to be controlled in order to achieve a low impact between the stops and Part A.

Control Jaw Movement

We examined the nest, specifically the jaw, to determine a method to control jaw movement and the displacement needed to control product alignment. The current nests used on the assembly machines do not have rollers but were designed to have one. For the linear cam design we are proposing, the rollers must be put back on the nests. As shown in Figure 17, the jaw is on a pivot and the reattached roller is at a distance h from this pivot.

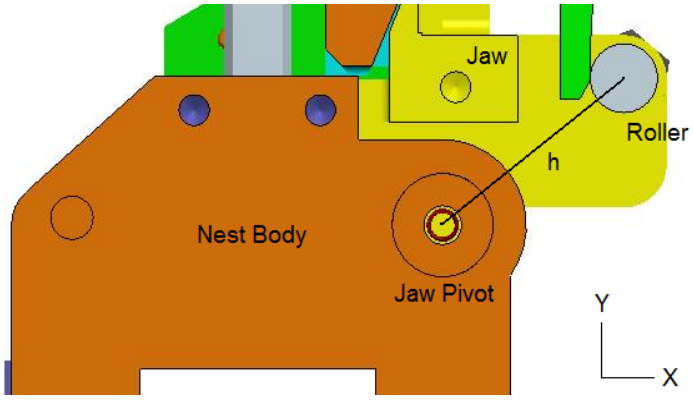

Figure 17: Jaw Roller Model Screenshot

The jaw rotates open and closed around this pivot, but for the linear cam design the jaw is controlled to only open slightly. The distance that we were concerned with was in the x direction

that is indicated in the figure. We wanted to limit the jaw to 0.010” in the x direction. This distance allows enough clearance for Part A to be placed on the nest to overhang the front of the break pad. The distance was also small enough to minimize the impact between Part A and the jaw’s carbide stops when the nest jaw closes.

In Figure 18, an exaggeration of the jaw movement as well as the important dimensions necessary for calculations are shown. The distance from the pivot to the roller is constant and the difference between o’ and o is the 0.010” in the x direction. We used these inputs to calculate the starting angle θ and the final angle θ’.

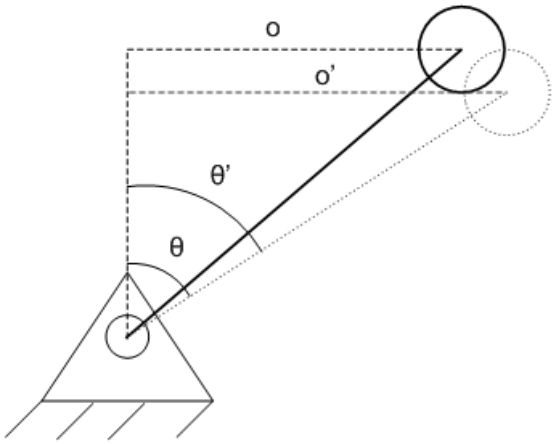

Figure 18: Jaw Roller Movement

We found the starting angle to be 51.602° when the jaw is closed and the final angle to be 52.712° when the jaw is open the 0.010”. These values are used later in the section discussing the Dynacam model created for the linear cam surface profile. The surface profile of the linear cam could not be designed before the existing motion of the lift cam mechanism was calculated and analyzed.

Examine Lift Cam Timing

The SVAJ diagram of the lift cam was examined to determine what section of the cam’s profile had to be the focus. The SVAJ diagram in Figure 19 shows the displacement, velocity, acceleration and jerk diagrams for the lift cam. The timing of the movements can be seen in any of these four graphs, but the displacement graph is the best representation of when the cam rises,

falls, and dwells. The main area of focus was when the cam falls from 110 to 207 degrees and rises from 233 to 300 degrees.

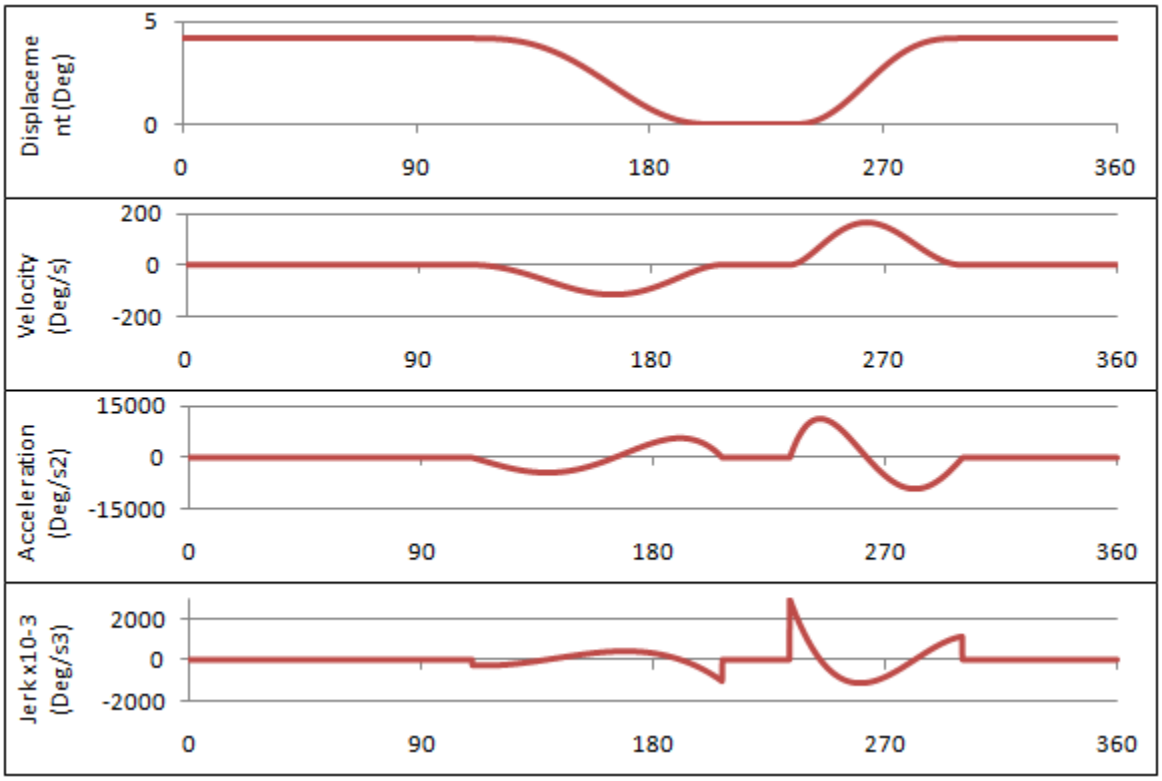

Figure 19: Lift Cam SVAJ Diagram

The cam's fall correlates to the fall of the pick-up head, or lift cam's end effecter, and the rise correlates with the rise. These two motions are important because this is when the linear cam surface makes contact with the roller on the nest. Since the goal was to control the velocity of the jaw, our focus was shifted to the velocity diagram of the lift cam.

The velocity diagram of the lift cam is shown in Figure 20. As stated earlier, we were concerned with the rise and the fall motion but after further investigation the focus was narrowed to just the rise. The reason for this focus was because the rise happens with a greater velocity. This motion also corresponds to the linear cam leaving the nest (the closing motion of the jaw), which was the motion of interest. The circled area in Figure 20 shows the general region on the rise when the linear cam would make contact with the roller on the nest jaw. Since the velocity profile had a direct connection to the velocity in which the jaw was opened and closed, the velocity profiles of the existing motions in this region had to be calculated and examined.

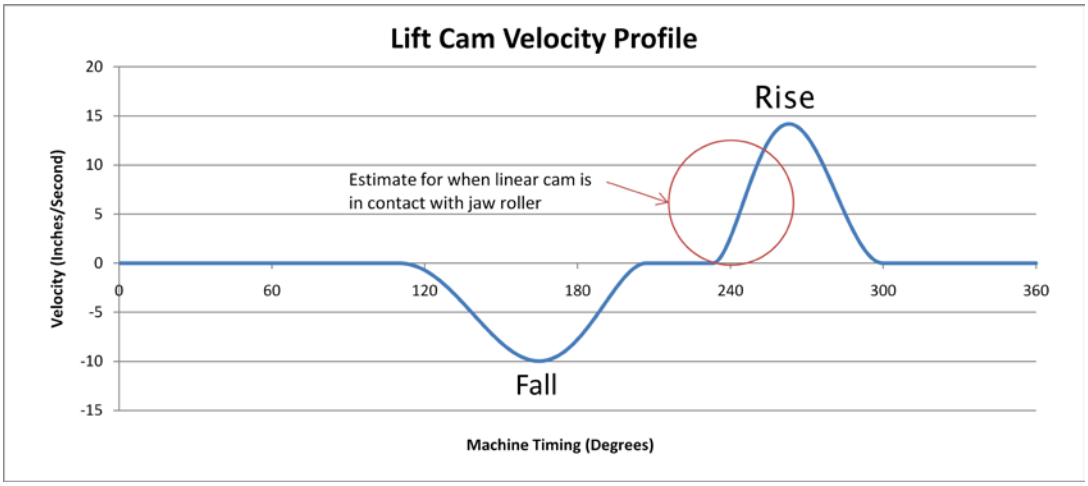

Figure 20: Lift Cam Velocity Diagram in inches per second

Velocity Profile Calculation

The camshaft that controls the lift cam rotates at a constant speed but the linear velocity that it produces on the roller follower is constantly changing in relation to the cam's profile. To understand this velocity profile described in Figure 20, calculations were made using the data that describes the cam's profile. Since our focus was the rise, the velocity during this motion on the lift cam was computed using the polynomial position function and the corresponding coefficients that describe the rise on the cam's profile. The velocity function for the cam's rise was computed by taking the derivative of its position function and multiplying it by the speed of the cam shaft. The output was multiplied by a conversion factor to convert the output velocity from degrees per second to inches per second. This output describes the linear velocity of the roller follower attached to the lower lever arm. This velocity profile for the total rise is shown in inches per second in Figure 21. This graph is of the rise region from Figure 20.

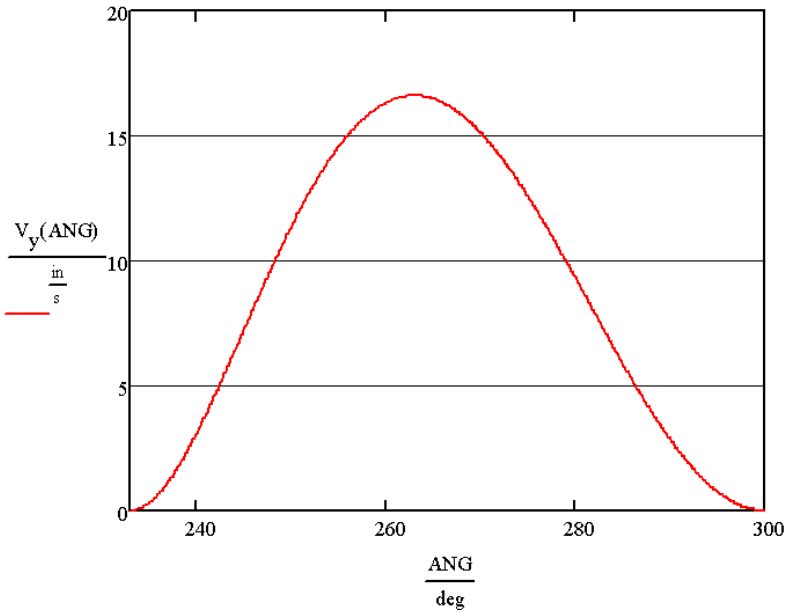

Figure 21: Velocity Profile of Lift Cam during the Rise

The motion of the pick-up head is directly related to the motion of the lower lever arm through a set of defined links. We can assume that the movement of all the links in the mechanism are linear because of the small angular distances that they travel. This assumption allowed us to calculate the velocity of the pick-up head by using the link ratios which are described in Figure 22.

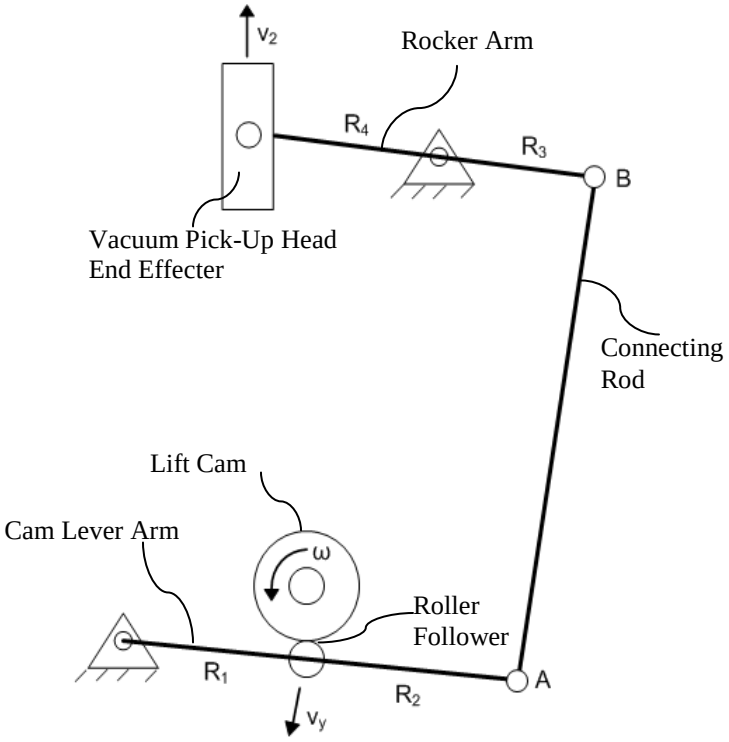

Figure 22: Links and Ratios

Because we assumed that the angular motions were small, the assumption was made that the velocity at point A was the same at point B. Applying these assumptions, the output profile was simply a scaled version of Figure 21 after applying the set of link ratios. We calculated this output by finding the angular velocity, $\omega_{lower,}$ of the lower arm. We used the equation for velocity, $v = r\omega$.

The velocity profile of the roller follower was used to find the ω_{lower} of the lower lever arm during the rise on the lift cam. We were then able to find the velocity profile at point A by using this ω_{lower} and the sum of R_1 and R_2 as the radius. This gave us the velocity profile at point B using the assumption stated earlier. The ω_{upper} of the upper rocker arm was calculated using the velocity at point B and R_3, this value allowed us to calculate the velocity profile of the pick-up head using this ω_{upper} and R_4. The output velocity profile of the pick-up head during the rise is shown in Figure 23. This ratio method was checked using the Dynacam linkage analysis software to find the velocity profile of the end effecter. We superimposed the two profiles to find any errors in our calculations and after comparison the ratio method showed to be correct.

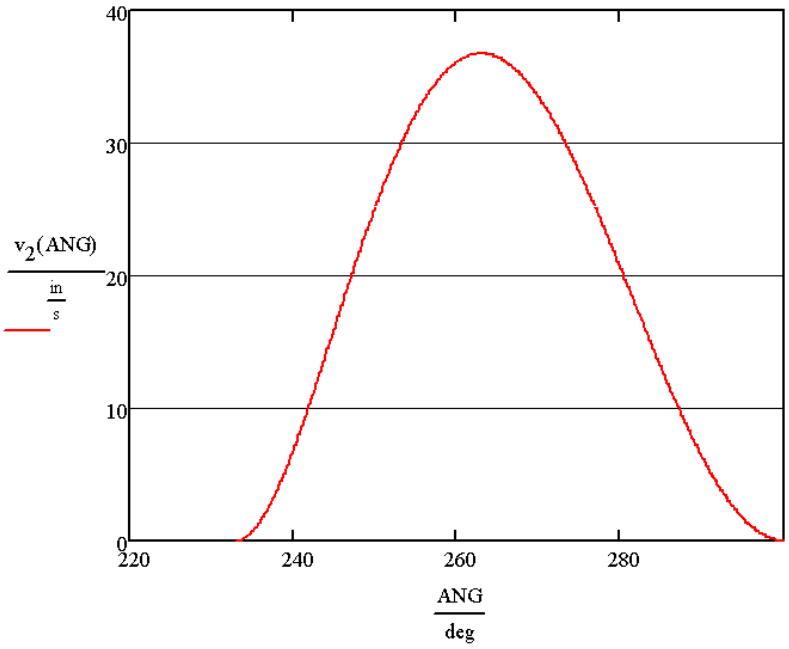

Figure 23: Velocity Profile of Pick-up Head during the Rise

We understood that during the rise motion the pick-up head mechanism was in contact with the nest for a portion of the total rise. Since we were considering the rise we knew that at the beginning of the velocity profile curve the mechanism was in the nest with zero velocity. We needed to create dimensions for the linear cam in order to determine when in the rise motion the linear cam surface and the roller on the jaw would no longer be in contact. The portion of the pick-up head velocity profile we used was determined by finding the angle corresponding to the time these two parts separated.

Linear Cam Measurements

The measurements of the linear cam were determined when the pick-up head was in contact with the nest. Although the nest is secured to the raceway, it still has the ability to move slightly along the indexing axis. This movement is there to make up for the tolerance between all the nests on that particular machine. It also allows for the shot pins to adjust and align the nest into the proper position before the functions of that station take place. The lengths of these pins were taken into account when designing for the length of the linear cam. Since the shot pins align the nest to a known position, the linear cam surface could not touch the roller surface until the nest's alignment was controlled by these pins.

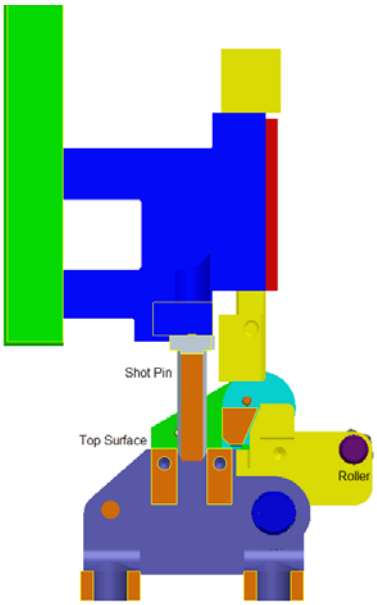

Figure 24: Cross Section of Shot Pins 0.100” in the Nest

We wanted to find a value that would allow the shot pins to enter the nest far enough to secure and align the nest before the linear cam hit the roller. We also wanted to make sure there was enough length for the linear cam surface to perform its function. The distance from when the shot pins break the plane of the top surface on the nest to the bottom of the stroke is 0.317”. We allowed the shot pins to enter the nest 0.100” before the linear cam touched the roller. This allowed the 0.070” chamfer and 0.030” of the flat on the shot pin to enter the nest. The pins in the nest can be seen in Figure 24. The center of the roller on the jaw is located 0.010” below this top surface. Therefore, the total length for the linear cam surface will be 0.227” and the total length of the linear cam will be 0.091” shorter than the bottom surface of the shot pins.
This dimension for the linear cam length allowed us to calculate when in the rise motion the linear cam surface will leave contact with the roller surface. Using our CAD assembly model of the station, we were able to set the shot pins into the nest the desired 0.100”. This position corresponds to the exact time when the linear cam would break contact with the roller during the rise, or the pick-up head leaving the nest. After setting the shot pins in place we were able to find the angle on the lift cam in which it occurs. The angle found from this process was 256°. We were now able to focus all of our calculations within the window from machine 233° to 256° during the rise motion. The trimmed velocity profile of the pick-up head is shown in Figure 25. This was referred to as the input velocity to the linear cam.

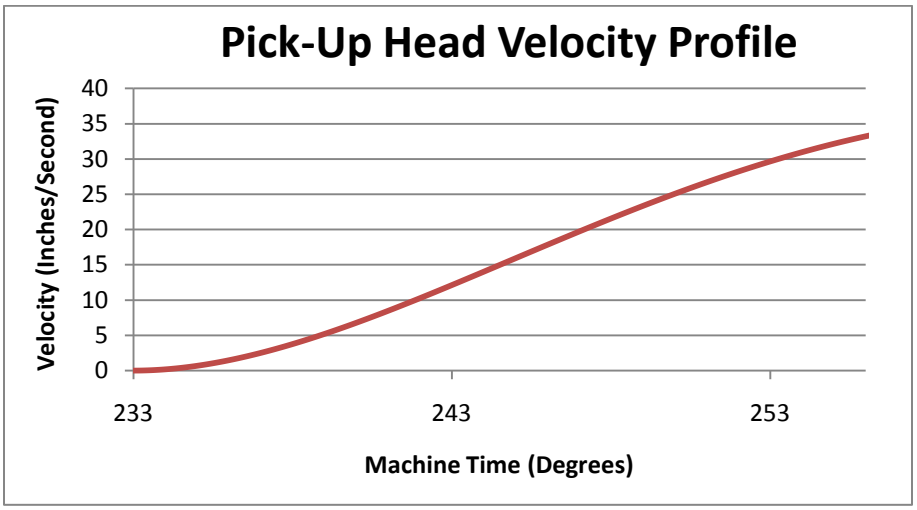

Figure 25: Velocity Profile of the Pick-Up Head from 233° to 256°

The focus was on the end points of this velocity profile segment. The goal was to control the velocity through the entire linear cam motion but more importantly to control the velocity at the start of the rise and at the point when the linear cam and the roller break contact. From this figure we saw that the motion was controlled at zero at the beginning of the rise but not at the end. The exit velocity was approximately 33 inches per second which we were able to control to zero by creating the linear cam surface.

Linear Cam Surface

After determining the output velocity of the pick-up head, we could design the surface profile of the linear cam. We were able to create an intricate velocity curve for the linear cam surface by using a spline function. This spline allowed us to manipulate and control the velocity profile for the linear cam surface. As described earlier, the goal was to have the roller leave the linear cam with a zero velocity to minimize impact between the stops and Part A. As shown before in Figure 25, the velocity profile of the pick-up head is shown starting at the end of a dwell prior to the rise motion with zero velocity. The velocity increases in a polynomial fashion as described by the position function that controls the rise in the cam profile. Since this vertical motion directly correlated to the rotational movement of the jaw through this spline surface, manipulation was necessary in order to create the output velocity we desired for the roller.

Since we wanted zero velocity at the beginning and end of the linear cam rise, we had to control both ends of the linear cam velocity profile. We set the velocity, acceleration, and jerk boundary conditions at either end of the curve to zero and the displacement was controlled by the angles at the start and the finish which were stated in the nest jaw movement section. We created a fifth order spline which gave us three interior knots to control the spline curve to the desired shape. As shown in Figure 26, two of the interior knots favor the left side of the graph which increases the velocity and the acceleration at the beginning of the motion. Since the input velocity of the pick-up head starts at zero we were able to make this sacrifice allowing more time to control the velocity profile back to zero at the end of the motion.

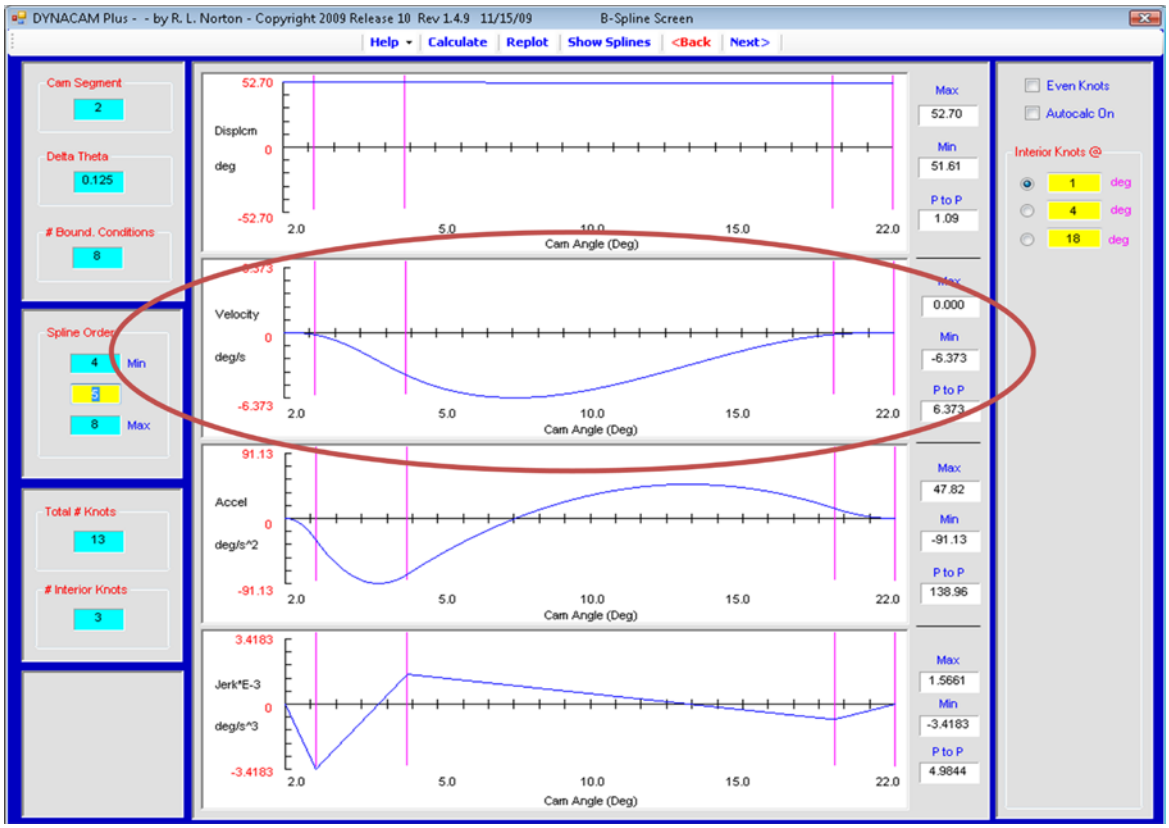

Figure 26: SVAJ Diagram for Linear Cam Spline Profile: Dynacam

The velocity profiles of the linear cam spline and the pick-up head are shown in Figure 27. The linear cam spline velocity profile corresponds to the primary vertical axis on the left while the pick-up head velocity corresponds to the secondary axis on the right. These are the two input functions that were used to calculate the output velocity profile for the nest jaw roller.

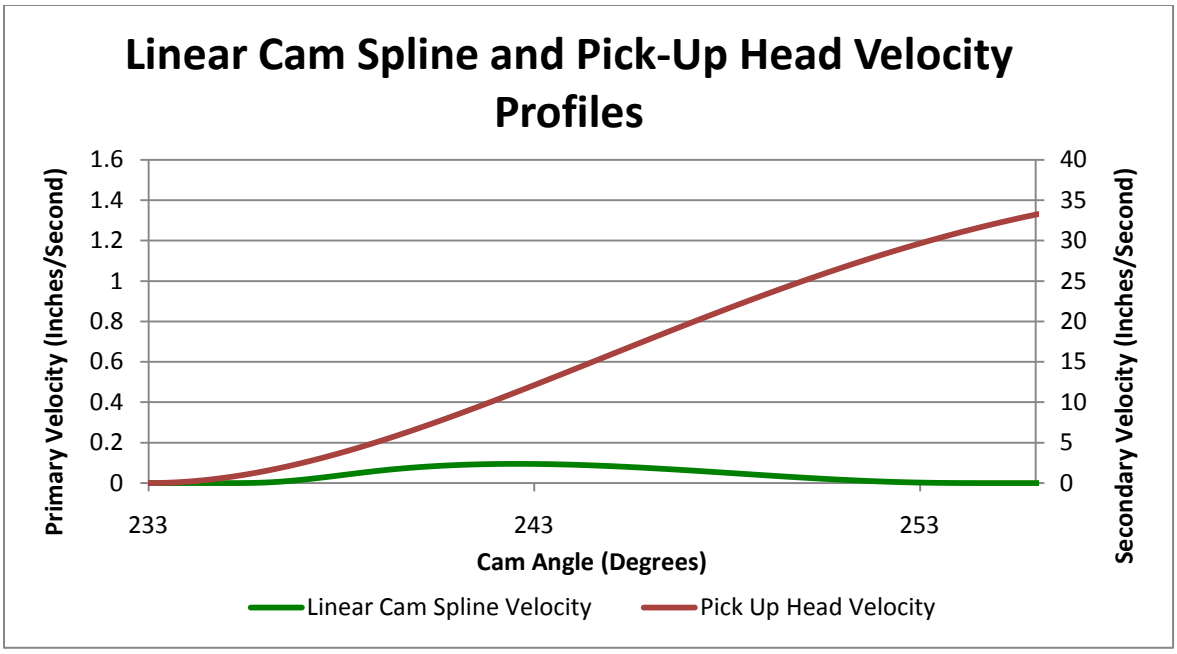

Figure 27: Linear Cam Spline and Pick-Up Head Velocity Profiles

The two curves shown in Figure 27 can be described using Figure 28 below. The pick-up head velocity profile was considered to be the input velocity v_2 which was the input to the linear cam. The linear cam spline velocity input was considered to be the instantaneous slope labeled as slope in Figure 28. Therefore, the product of these two curves produced the output roller v which was the velocity profile we desired.

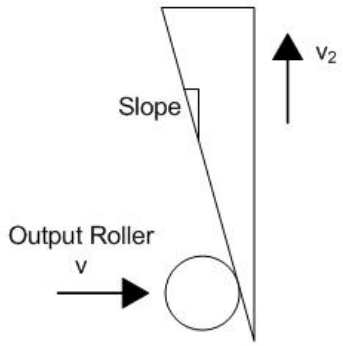

Figure 28: Motion of the linear cam and roller

The three velocity profiles are shown in Figure 29. The nest jaw roller velocity and linear cam spline velocity are shown on the primary velocity axis, while the pick-up head velocity is shown on the secondary velocity axis. The jaw roller velocity profile was described as the output roller v in Figure 28. This curve shows that the output velocity of the roller is

controlled to a max value of about 1.3 inches per second with both ends of the curve controlled to zero velocity. The velocity calculations behind the linear cam design are detailed in Appendix D. Since this was the shape that we desired for the velocity profile of the nest jaw roller, we were able to move forward by exporting the surface profile coordinates of the linear cam.

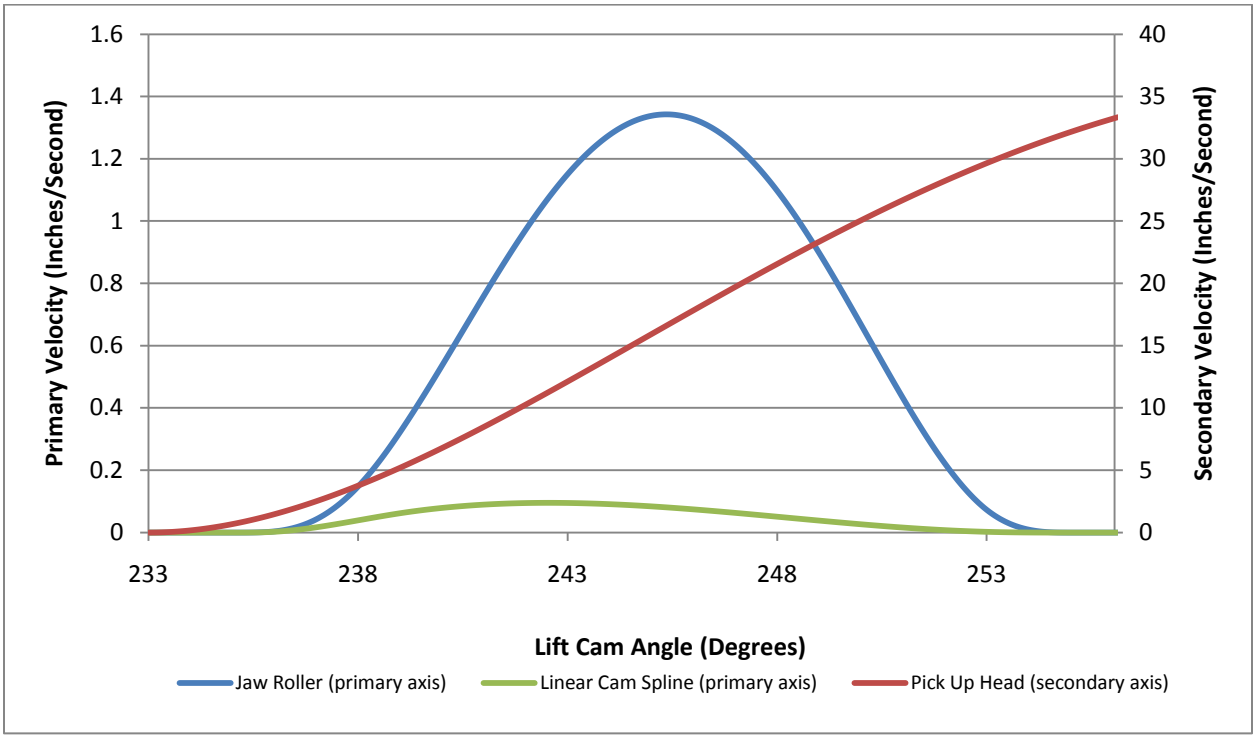

Figure 29: Velocity Profiles of the Roller Follower and the Vacuum Slide

The x and y coordinates of the linear cam spline surface profile where exported into Microsoft Excel and normalized to start at the origin. The spline normalized at the origin can be seen in Figure 30 (a). The point values were then used to create the spline in ProEngineer creating the cam surface for the linear cam. This can be seen in Figure 30 (b). The creation of a long dwell at the top of the spline allowed for the pick-up slide to over travel completely and still ensures the nest jaw roller never makes contact with the angled surface at the top of the spline. A chamfer was added to the bottom of the linear cam to make up for inconsistencies between the nests. The chamfer was also given the same geometries of the shot pins to eliminate large impacts between the linear cam and the roller. Appendix A shows the drawing of the linear cam. The exact spline curve can be found in the cad model in Appendix F.

a)

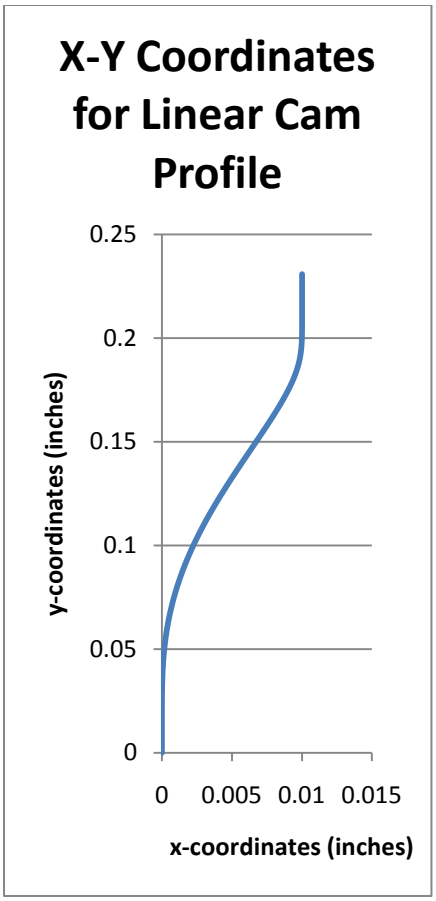

b)

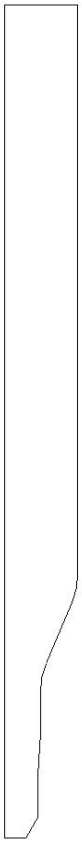

Figure 30: (a) x-y Coordinates for Linear Cam Profile **(b)** Final Linear Cam Design side profile

The linear cam and its surface were complete but a design to attach and locate the linear cam in the correct orientation in relation to the nest jaw roller was still necessary. The final piece to the complete design was to create the support or spacer piece to hold and position the linear cam in place.

Linear Cam Support

There were several ways to attach the linear cam to the existing mechanism. We needed to position the linear cam surface in the correct location in relation to the roller and the shot pins. The linear cam also needed to be placed completely vertical to ensure that the function we desired would be achieved. The constraints for the design were to use existing holes and geometries, not change the existing tooling, and not interfere with any existing motion. The part could have been designed in a one part or two part design, both having pros and cons. The one part design would be the linear cam and its support designed and machined together as one and

the two parts would be them designed as separate parts. The one part design would work best to eliminate the tolerance issues that we would encounter with a two part design. The negatives for the one part would be machining the intricate geometry out of hardened tool steel especially if the part needed to be replaced. The two part design allowed for the spacer or support for the linear cam to be made out of a common tool steel. The cam would be machined out of hardened tool steel but if a replacement was necessary the whole tool did not have to be replaced.

We designed the new tooling to be two separate parts that would use the existing geometries and holes on the mechanism to locate and attach. In Figure 31, the linear cam and the support piece are shown. The pink piece represents the design for the support piece; this support utilizes the existing holes for attachment as well as the top surface of the pick-up housing to locate. This surface will locate the part in the vertical direction as well as insure the part's perpendicularity. There are also two slip fit dowel holes that will control the location of the linear cam in relation to the support.

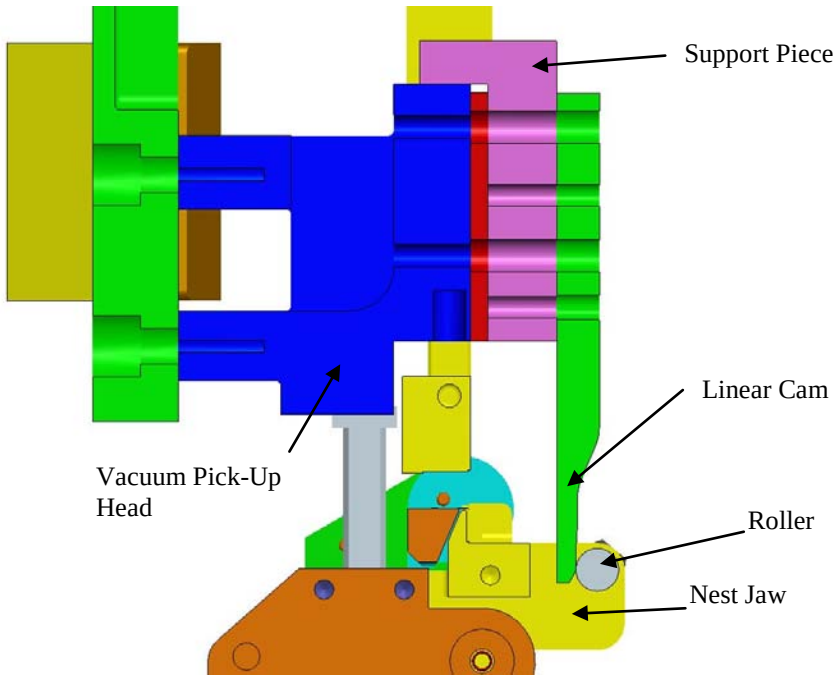

Figure 31: Linear Cam Mechanism Cross Section

The final design for the linear cam support is shown in Figure 32. The prototype design allowed for the support to fit over the existing slide retainer gib but the final design included the

slide retainer volume in the support. This was done to eliminate a tolerance between the slide retainer and the support. Appendix B shows the drawing for the linear cam support.

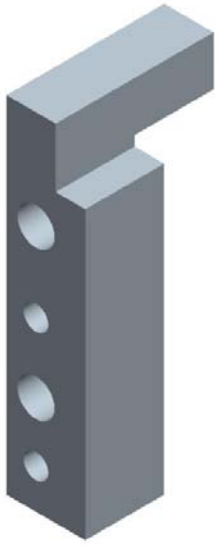

Figure 32: Linear Cam Support (Isometric View ProEngineer)

Linear Cam Final Design and Testing

The final linear cam design including the support and the linear cam is shown in Figure 33. The support is attached to the two existing holes and located off the top surface of the pick-up housing. The support includes the dimensions of the slide retainer which eliminates the retainer on the left side of the housing. The linear cam and its support does not interfere with any of the existing motion of the machine and is small and compact allowing for it to fit within the existing confines of the station.

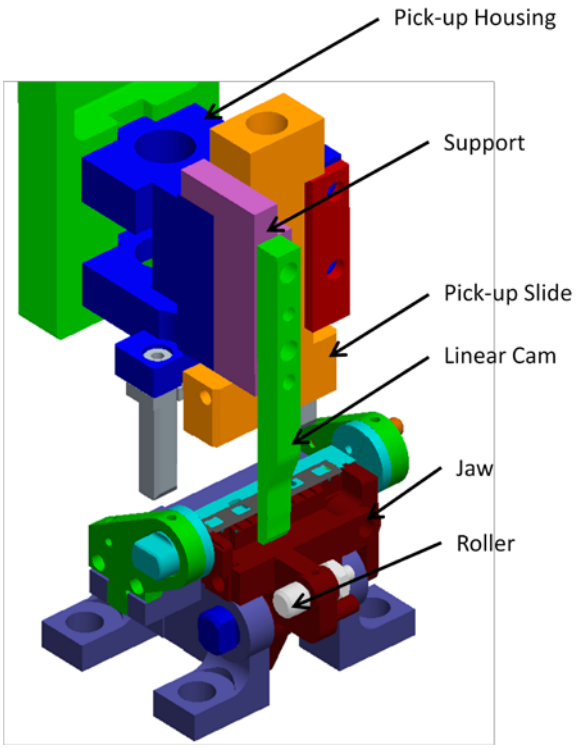

Figure 33: Final Linear Cam Design (Isometric View ProEngineer)

After confirming the dimensions and the kinematics of the nest jaw movements using ProEngineer software, the linear cam and support were sent to be manufactured. We used these manufactured parts to test on production machines at the plant. Testing was done to measure vibrations of the nest or any impacts with and without the linear cam attached. The velocity of the jaw was measured by putting the linear cam and support onto the pick-up head mechanism as well as the roller back on the nest jaw. The movements of the jaw were checked visually in a prototype lab before moving the parts to the production machine on the floor.

Transfer Cam Redesign

The cam design method has improved immensely from previous years. The first cams were designed by hand-plotting displacement versus angular cam rotation. By using a French curve the points were connected to form the cam profile. More recently, cam design shifted its focus from displacement curves to acceleration curves. Designing a cam by the acceleration profile allowed the designer to obtain the displacement curve through integration. In today's

industry, more emphasis is placed on the acceleration profile because slight modifications to the acceleration profile can result in large changes in the system's dynamics.

The overall goal of cam design is to control the motion of an end effecter through a follower train. Producing a mechanism with low kinetic energy requires the peak velocity of the cam to be minimized as:

$$KE = \frac{1}{2}mv^2 \tag{15}$$

If the dynamic forces of the mechanism are the focus of reduction then the peak acceleration of the cam should be minimized as $F = ma$.

To produce a cam with minimal vibrations the jerk function should be finite. Jerk is defined as the time derivative of the acceleration function. Because all of these functions are related through derivatives or integration, there exists a tradeoff between optimizing each cam profile function.

Before any redesign work could be completed, the existing transfer cam was analyzed in Dynacam. Once in Dynacam the velocity, acceleration, and jerk functions were examined. It was also essential for the timing and function of the cam be studied to ensure function was not compromised in the system. Figure 34 depicts the timing profile of the transfer cam.

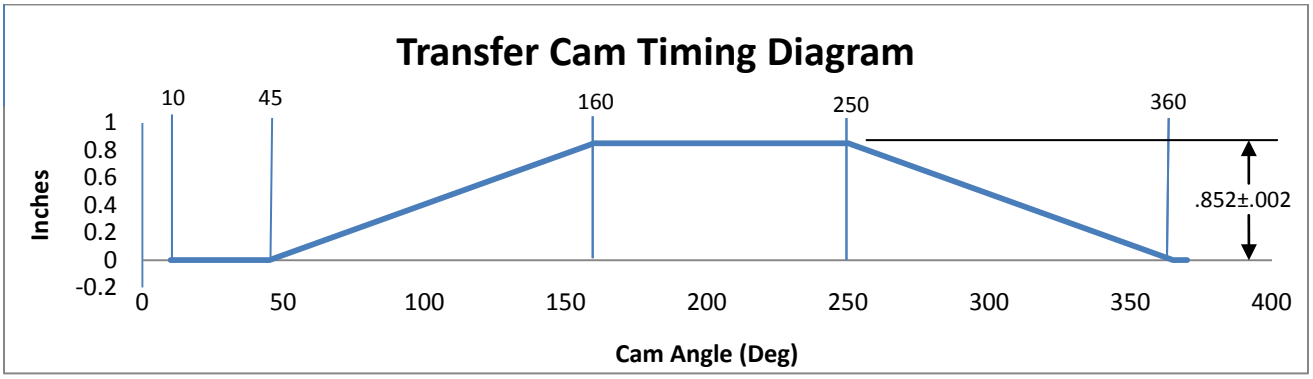

Figure 34: Transfer cam timing diagram

The transfer cam moves the linkage to slice Part A from the magazine and position the Part A over the nest, on top of Part B. At machine zero, when all camshafts are aligned with their keyways in the vertical position, the transfer cam is finishing a fall motion profile. Following the fall, the cam begins the shorter 35° low dwell. The low dwell represents the time the transfer is away from the nest and is waiting to pick out another Part A. The next section is

the 115° rise where the slice bar moves towards the nest and pulls Part A out from a stack. At the 90° high dwell, the slide makes contact with a hard stop and is held against it until the vacuum head lifts Part A off the slide. The last fall segment represents the transfer retracting to its original position, away from the nest.

To further understand how the existing cam operated, kinetostatic and dynamic force and vibration analysis were conducted. The same tests were conducted on the optimized spline cam to compare the results. Figure 35 illustrates the kinetostatic force comparison between the modified trapezoidal and spline cams. To ensure the cam follower does not lift off the cam, the forces must be above zero. The kinetostatic force comparison shows both cams sustaining a positive force; therefore, the optimized cam can effectively operate without cam liftoff. Cam liftoff is when the roller loses contact with the cam surface; therefore, the system stops functioning. The positive force is attributable to the air cylinder in the system holding the roller onto the cam.

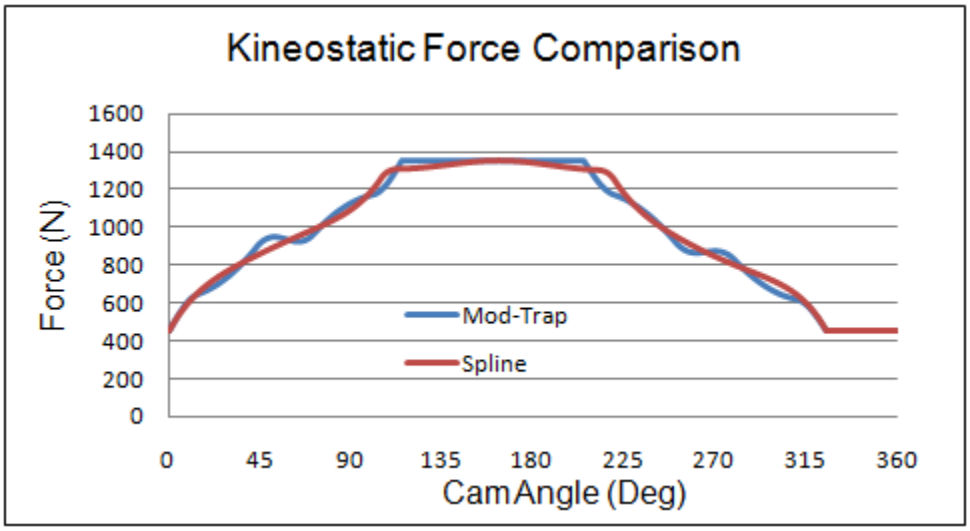

Figure 35: Kinetostatic force comparison

The dynamic force represents the system with its spring constant applied. Figure 36 portrays how the system actually acts more accurately than the idealistic kinematic analysis.

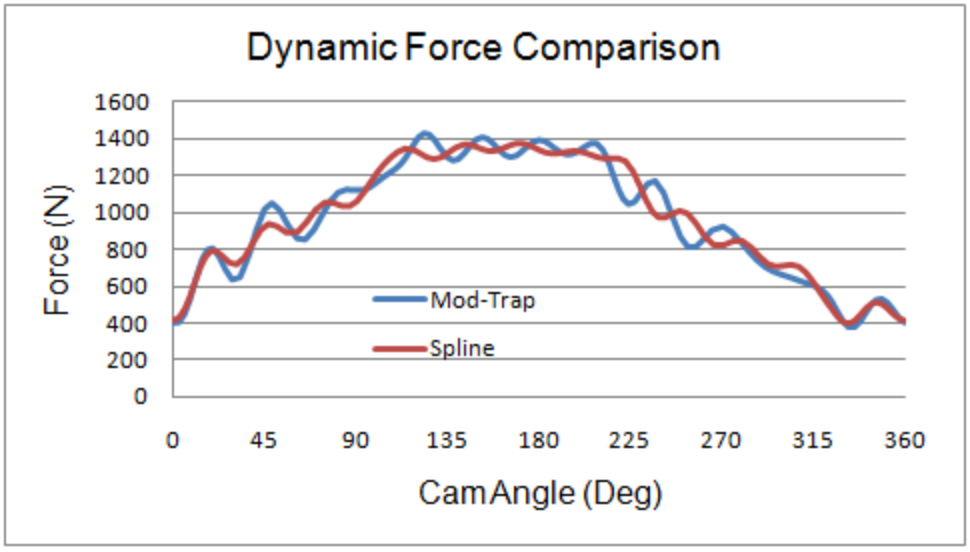

Figure 36: Dynamic force comparison

The kinematic and dynamic accelerations of the modified trapezoidal cam are overlaid and depicted below. Dynamic accelerations reveal vibrations in the system because the spring constant of the system is applied. The dynamic analysis, depicted in Figure 37, clearly shows the vibrations during the dwells, which accurately represents the system moving internally.

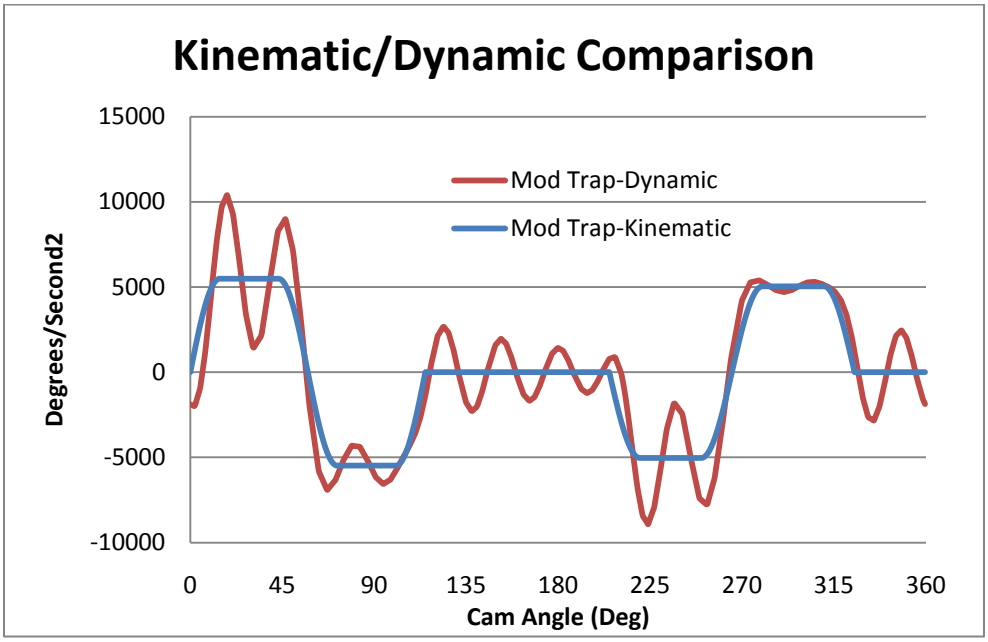

Figure 37: Transfer cam dynamic and kinematic accelerations

To optimize the cam profiles we looked at two different types of functions that are superior to the existing modified trapezoidal function. First were polynomial functions where boundary conditions are applied to the mathematical function to allow for continuous derivatives. The second set of curves is a series of spline functions that modify polynomial equations to enhance the motion curve as desired.

The polynomial functions provide flexibility in cam design by controlling a variety of motion and derivatives. Unfortunately, once a polynomial curve is formulated from boundary conditions and constants, the curve slope cannot be modified further. To supplement this, there are mathematically defined spline functions. Spline functions are piece-wise polynomial functions that are attached together at certain locations called "knots" and produce a continuous and smooth function curve. Polynomial function segments are blended together to produce a spline curve of order *n* and produce a continuous function. All the derivatives of that function are continuous to the *n*-2 derivative.

By introducing more knots, spline curves become very advantageous in the cam design process. As stated previously, knots are the endpoints of the polynomial segments that are blended together to produce the spline curve. By moving the location of the knots, the spline function slope changes without disrupting the location of the boundary conditions. This is a huge advantage in cam design because the knots can be moved until the desired motion is obtained.

For each spline curve, there must be at least one knot for each order of the spline at each endpoint of the spline and any remaining knot can be placed in between the endpoint. The number of polynomial segments that produce the spline curve is always one less than the number of knots. For example, a spline curve that has seven knots is produced from six polynomial segments. Spline functions are superior because they allow the designer more flexibility and control when making motion profiles. Higher order splines allow more derivatives to be continuous. This can be used to optimize cam profiles by changing the knot order and locations. In order to design an optimal cam profile in a limited amount of time an appropriate computer program is needed. Dynacam allows the user to select a B-Spline motion curve to design a cam. The desired boundary conditions are input to the program to determine the polynomial function of the spline. The following screen allows the user to either evenly distribute the knots or

customize the spline shape by moving the knots to any location. Utilizing this program we were able to design an optimized transfer cam.

The current transfer cam profile is defined with a modified trapezoidal function. These types of functions are outdated because there is less control of the acceleration profile of the cam. For more control of the acceleration profile, we chose to use a spline profile. We redesigned the cam as a two section cam. The first section is defined by a 325° spline function with a pseudo high dwell. The second section is the low dwell for the remaining 35°. In this case the high dwell can be approximated using a spline function because of the over travel in the system. The pseudo dwell of the spline cam is superimposed on the modified trapezoidal cam in Figure 38.

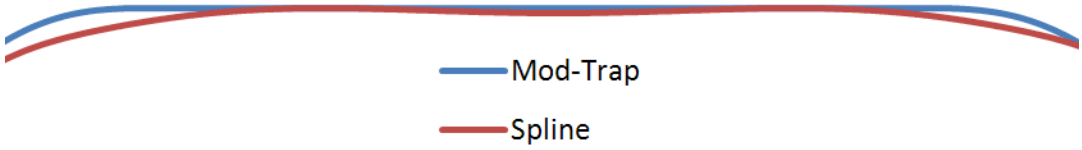

Figure 38: Pseudo Dwell

Over travel in the system ensures the slice bar is always in contact with the hard stop. Consequently, the slice bar is always in a known position for product pick-up. However, the over travel results in large impact forces within the system. This large force is one of the motives for optimization of the existing cam.

The first step in the iterative process was selecting the sections of the cam. Program Dynacam makes it simple to create a cam by specifying angular sections of the cam and what motion is desired for each of the sections. Implementing a pseudo dwell allowed us to combine the first three cam segments into one spline because our spline function incorporated first a rise, then the pseudo dwell, and finally a fall, leaving only the 35° dwell at the end of the cam cycle.

Table 7 – SVAJ input values for the redesigned transfer cam

β	Start	End	Motion	Program	Initial Position	Final Position
325°	0°	325°	Spline	B-Spline	0°	0°
35°	325°	360°	Dwell	Dwell	0°	0°

The boundary conditions are critical in the optimization of this cam. Because of the violent collision with the hard stop at the end of the rise, before the high dwell, the velocity profile had to be controlled. The velocity profile is subject to minimization because impact force and velocity are directly proportional. In order to reduce the large impact force at this instant the velocity must be lower. Impact force is defined approximately as equation 14.

$$F_i = v\sqrt{\eta km} \tag{14}$$

Impact force is defined with velocity, a correction factor η=1 assuming dissipation is negligible, equivalent spring constant and equivalent mass of the system as variables. Using the spline function in Dynacam, velocity was controlled. Selecting a low velocity boundary condition before the high dwell resulted in a lower impact force. A trade off for the lower velocity is a slight increase in acceleration, but the focus of the optimization was to reduce the harsh impact.

Table 8 -- Spline boundary conditions

Dynacam Boundary Conditions						
θ	**0°**	**115°**	**135°**	**190°**	**210°**	**325°**
s	0	8.0535	8.143	8.143	8.0535	0
v	0	13	0	0	-13	0
a	0	--	--	--	--	0
j	--	--	--	--	--	--

To ensure the position of the slice bar, a 20 thousandths of an inch over travel of the slider was built in the design. This over travel is necessary for the precise location of Part A for pick-up by the vacuum head. The over-travel in the system also results in the large impact force. To make the existing system have less of an impact, it was essential to determine the corresponding cam displacement to slice bar displacement. Determining the equivalent cam displacement of 20 thousandths in slice bar displacement gives the position that the velocity needed to be constrained. The lowest value the velocity could be reduced to without significantly effecting acceleration was 13 degrees per second.

In order to determine the corresponding cam angle over which the transfer cam made contact with the hard stop for our boundary conditions a cam follower calculator in an Excel worksheet was used along with a simple ratio. The Excel worksheet takes follower information

and changes the displacement of the cam into a degree value. The ratio of distance per degree was used to find the degree that corresponds to the 20 thousandths before impact.

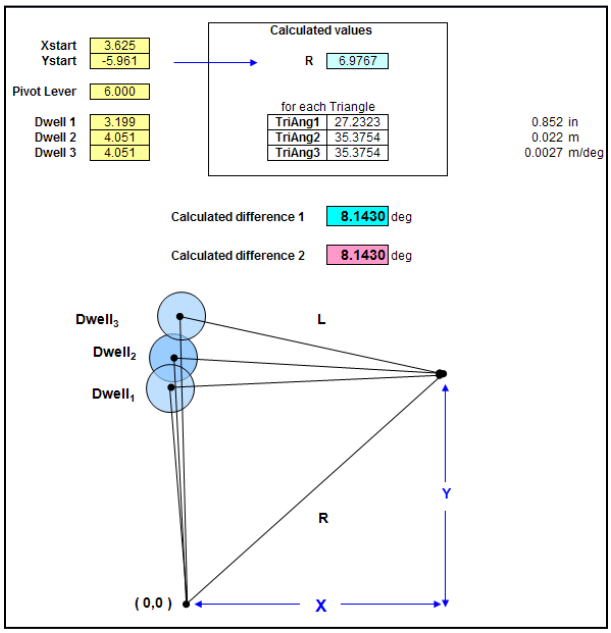

Figure 39: Cam follower calculation

$$\frac{\boldsymbol{Cam\ Displacement\ at\ 20\ thousandths}}{Total\ \ Cam\ \ Displacement} = \frac{Total\ \ Stroke\ -20\ thousandt\ \ hs}{Total\ \ Stroke\ \ of\ \ Slice\ \ Bar} \tag{15}$$

$$\frac{\mathbf{8.0535}}{8.143} = \frac{1.818 - .020}{1.818}$$

The solution to the ratio in bold shows the corresponding cam displacement was 8.0535 to the total displacement of 8.1430 of total cam displacement. With this value known the velocity profile could be controlled at that instant to reduce the impact force in the system. Because velocity directly affects impact force the reduction in velocity from 31.48 degrees per second to 13 results in a 58.7% reduction in impact force. With the velocity profile defined the next step in the iterative process was moving the spline knots to reduce the acceleration profile. Controlling the acceleration was still necessary to reduce forces in the system, shown in Figure 40.

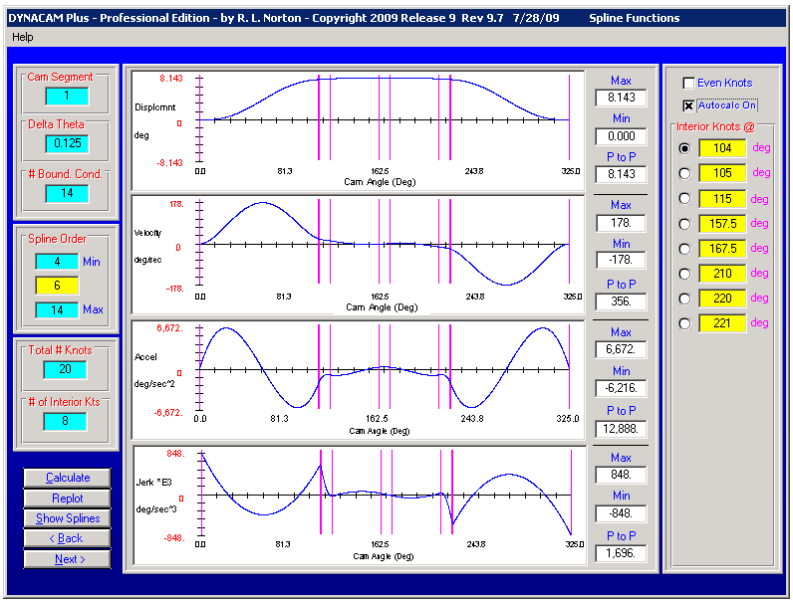

Figure 40: Spline profiles for the redesigned transfer cam

Moving the knots incrementally we found the best arrangement to reduce the acceleration profile.

With the profiles of the cam complete, the output of Dynacam was used in Excel to visually compare the existing and optimized transfer cam acceleration profiles. The relative magnitudes of the graphs are the focal point of analysis. The peak accelerations of the spline cam are greater to make up for the lower velocity at impact. Figure 41 illustrates the kinematic acceleration comparison between the modified trapezoidal cam and the spline cam.

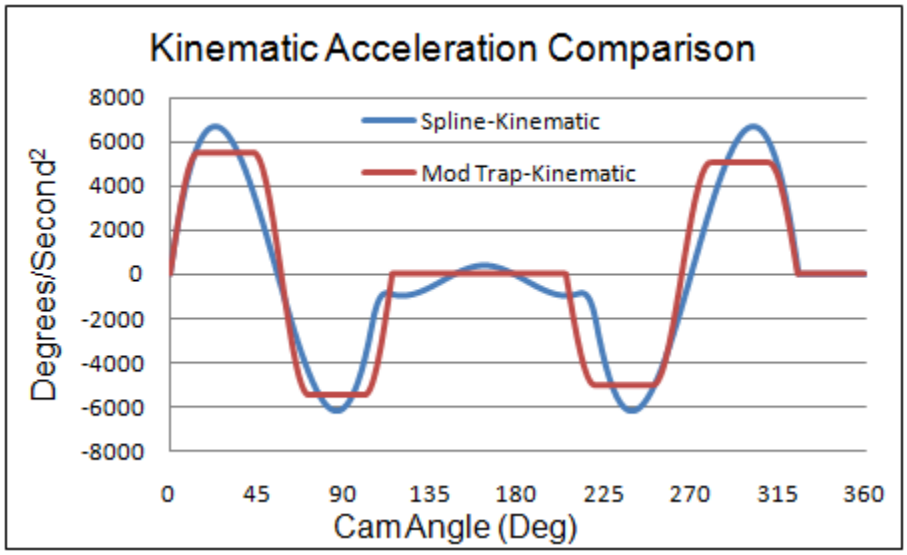

Figure 41: Spline v. Mod-Trap kinematic acceleration comparison

The dynamic acceleration comparison in Figure 42 shows the existing cam and optimized cam having the same vibrations because the same spring constant and dampening coefficient were used; however, the peak amplitude of the spline cam acceleration is lower than the existing cam's peak acceleration. Also, the overall acceleration during the high dwell is lower even with the spline cam's pseudo dwell. During the fall of the cam, the spline has a higher acceleration because of the rapid change in velocity to reduce impact force. Since the velocity was reduced at that instant, the acceleration has to increase.

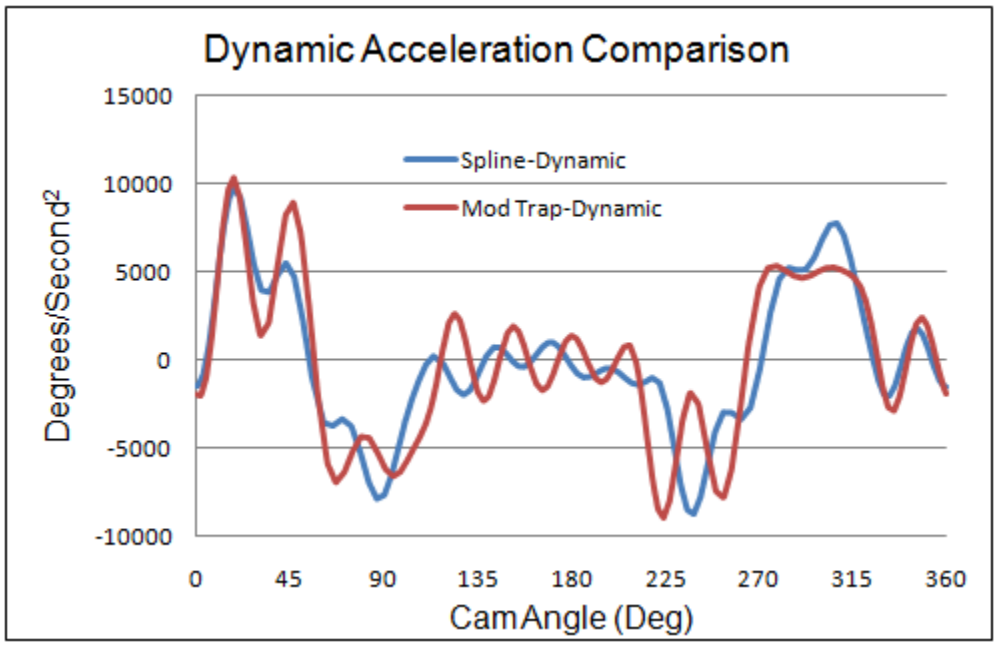

Figure 42: Spline v. Mod-Trap dynamic acceleration simulation comparison

VI. Results

Following the design and manufacturing of the linear cam and redesigned transfer cam, we performed experiments on the existing machines to compare to our calculations. High speed video footage, velocity and acceleration data were recorded on full speed production machines. The data and video were analyzed in order to draw conclusions on the validity of the designs.

Linear Cam Testing Results

Before testing our linear cam on a production machine, we tested its functionality at our sponsor's prototype lab. The linear cam and support were mounted on a hand crank machine in order to check the fit and motions of the manufactured pieces. A nest with the proper roller was set up in the index. After installation and adjustment of the station, the machine was hand cranked through a cycle several times. A simple visual check of the motions was performed to check operation before proceeding to full speed testing. The transfer station completed a full cycle with no interferences to existing motions. The linear cam contacted the roller at the beginning of the spline surface, just after the shock pins inserted into the nest. The jaw was opened a suitable distance and then closed on the rise of the pick-up head. Figure 43 shows the linear cam and support mounted on the machine, with the linear cam in contact with the jaw roller.

Figure 43: Linear cam and support mounted on transfer station

Velocity data of the jaw movement and high speed video footage of the linear cam function was collected on production machines at full speed. Velocity data was compared to the

calculated jaw velocity profile. Proper motions and vibrations were looked for in the high speed video. The linear cam and support piece were mounted and the jaw roller was installed on two consecutive nests. Data and video footage were taken of nests with and without rollers to establish a baseline.

High speed video footage was taken at 1000 frames per second for 1 second. This footage showed that on full speed machines, the linear cam engages the jaw roller and fully opens and closes the nest jaw. The jaw is gently closed and minimal jaw vibrations are visible in the video footage as the linear cam disengages. The shock pins can be seen entering the nest and locating the nest just prior to contact between the linear cam, ensuring that the linear cam will be properly located relative to the roller.

Linear velocity data of the vertical jaw movement was taken in sync with the video footage from a Polytec PDV-100 Portable Digital Vibrometer. The resolution was 125 mm/s / V with a maximum range of ±4 V or ±500 mm/s. This device had a low pass filter of 5 kHz and no high pass filter. This data is recorded on an oscilloscope that inputs to the high speed camera software. The software collected samples at 10,000 samples per second in sync with the 1000 frames per second video footage. So we get 10 samples for every frame of video footage.
The laser vibrometer measures the vertical velocity of the jaw on a point near the roller. Because the jaw only pivots about 1 degree, we adjusted the vertical velocity data to a horizontal velocity in order to compare it to the calculated velocity of the jaw. Since the roller and the laser point of measurement were very close and the angular displacement of the jaw is so small, we assumed the horizontal velocity at the laser point was the same as at the roller location, where calculated.

To convert this velocity vector, we simply used a trigonometric ratio. The horizontal velocity can be calculated using equation 16 and Figure 44 for reference:

$$V_X = \frac{V_Y}{\tan \theta} \tag{16}$$

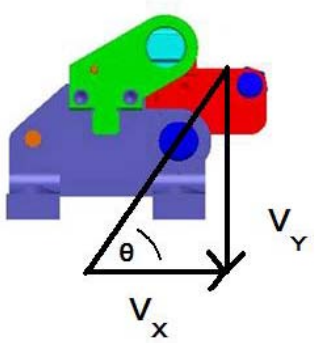

Figure 44: Profile of Jaw Showing Vertical to Horizontal Velocity Conversion

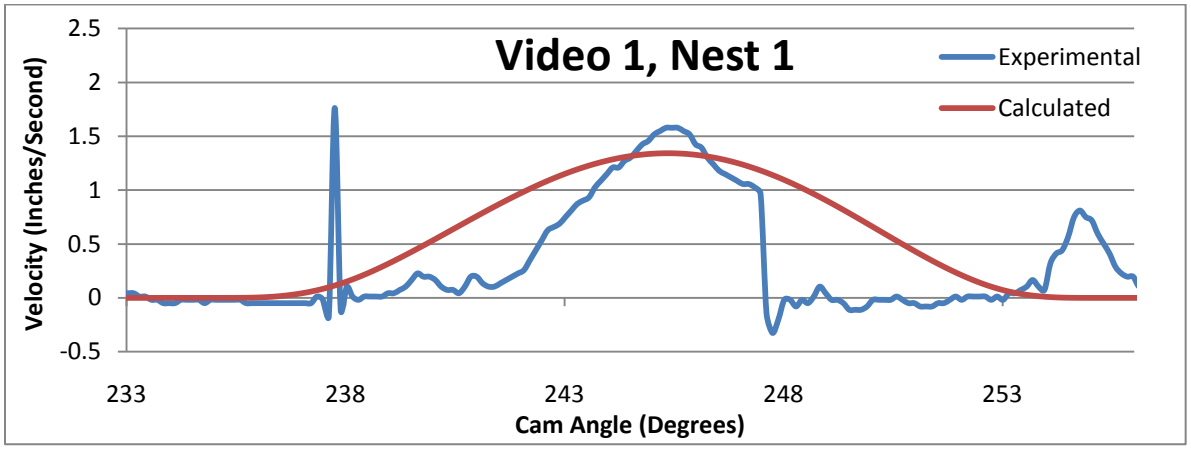

Figure 45: Jaw Velocity Comparison from Video 1 on Nest 1

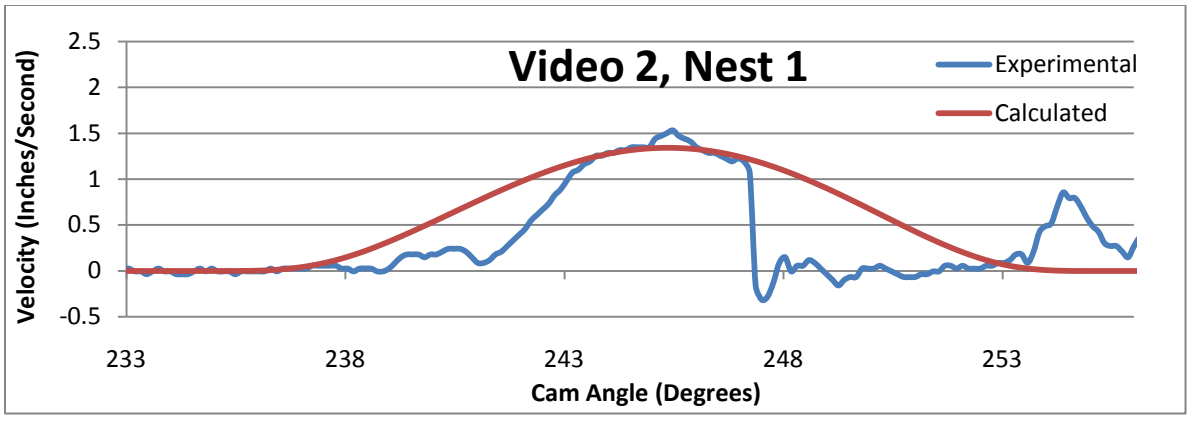

Figure 46: Jaw Velocity Comparison from Video 2 on Nest 1

Figure 45 shows the calculated velocity of the nest jaw with the adjusted experimental results overlaid. Figure 45 and Figure 46 are of the first nest on our test set up, from two different samples. The initial spike in Figure 45 is due to a small imperfection in the transition from the upper dwell to the spline surface, causing a short velocity spike. The shape and

amplitude of the experimental data fits the calculated bell curve. The drop off at 248° is due to the tolerance in the nest alignment. This nest is set slightly forward, so the linear cam does not contact the roller until it is slightly in already. As the linear cam exits on this nest, it guides the jaw until it closes, slightly earlier than expected. This error is more favorable than the alternative, which is shown in Figure 47 and Figure 48.

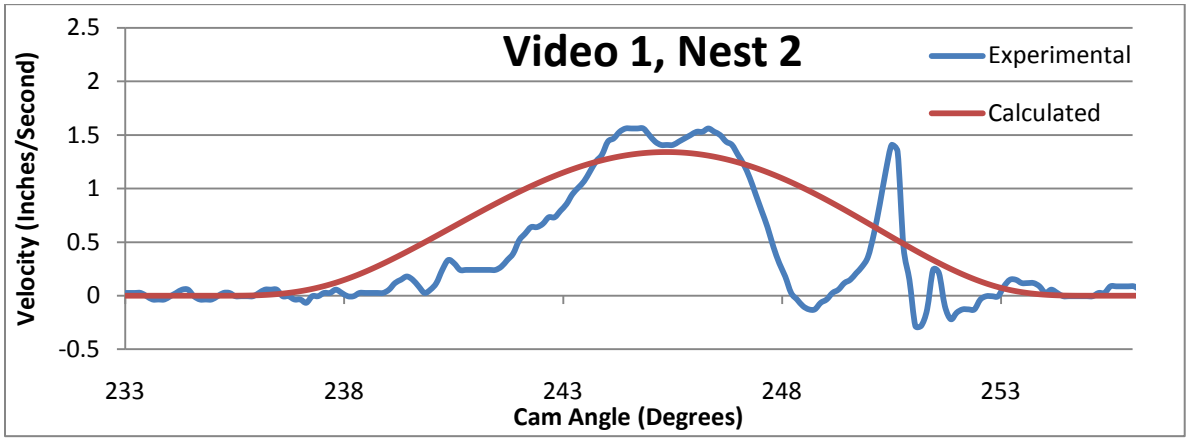

Figure 47: Jaw Velocity Comparison from Video 1 on Nest 2

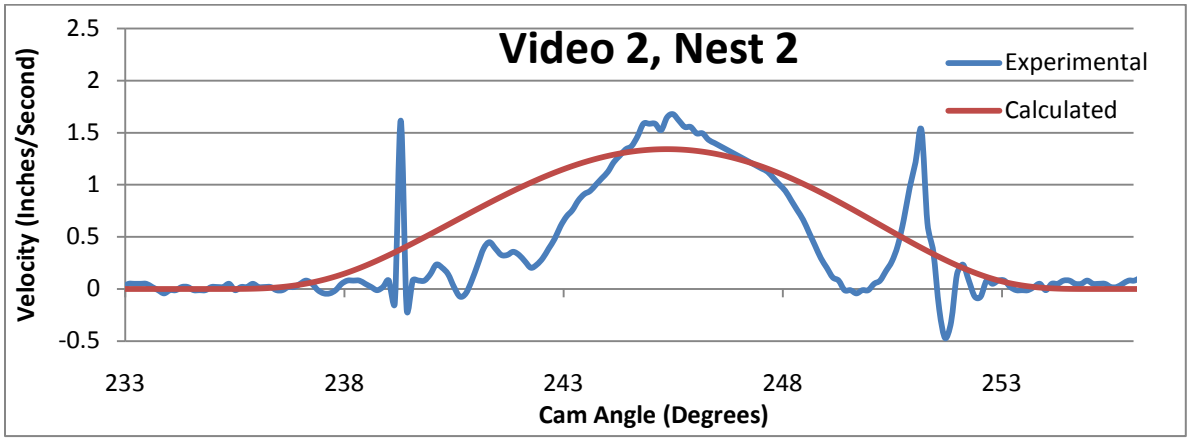

Figure 48: Jaw Velocity Comparison from Video 2 on Nest 2

From these figures, a similar curve is shown in the experimental data for the second nest on our test set up. However, in the second half of this motion, a sharp drop-off, followed by sharp oscillations can be seen. This is because this nest was slightly behind optimum, causing the cam to contact the roller earlier on the down stroke. When the lift motion begins, the cam lowers the jaw roller until it reaches the end of the linear cam. However, since this nest is behind slightly, once the roller reaches the end of the cam surface, it jumps on the rough chamfer we put

on the bottom of the cam and rams into the stops on the nest, bouncing slightly when it closes. This is not desirable, because the large accelerations due to bouncing could cause the product to slide out of alignment.

Figure 49: Linear Cam Profile Highlighting Design Change

In order to avoid large velocity and acceleration spikes from the discontinuous cam surface, the chamfer on the end of the part was removed. This is replaced with a spline similar to a fillet. This change is highlighted in Figure 49 The velocity and acceleration slope at that intersection point must be zero, which would be a boundary condition of the spline. This small change would reduce large velocities oscillations due to the jaw bouncing as it jumped off the linear cam when it reached the chamfer.

Transfer Cam Redesign

The goal of redesigning the transfer cam was to reduce the slice bar velocity before it came into contact with the hard stop. The impact force calculations are shown in Appendix E. Lowering the velocity would directly reduce the impact force of the system because velocity and impact force are directly proportional as shown in the following equation:

$$F_i = v\sqrt{\eta k m} \tag{14}$$

To reduce the velocity profile, boundary conditions in Dynacam were used to control the velocity profile and make it 13 at the point of impact with the hard stop. The dwell timing was not modified during the cam redesign to ensure proper function of the machine.

In order to quantify our results, acceleration data was collected on the machine with an accelerometer attached to the end of the slice bar. This data was used as our baseline to compare the spline cam acceleration to. Once the acceleration data was collected for both cams, the data was organized in a Microsoft Excel worksheet and averaged to obtain a reasonable outline of how both systems operated. The measured acceleration data is show below in Figure 50.

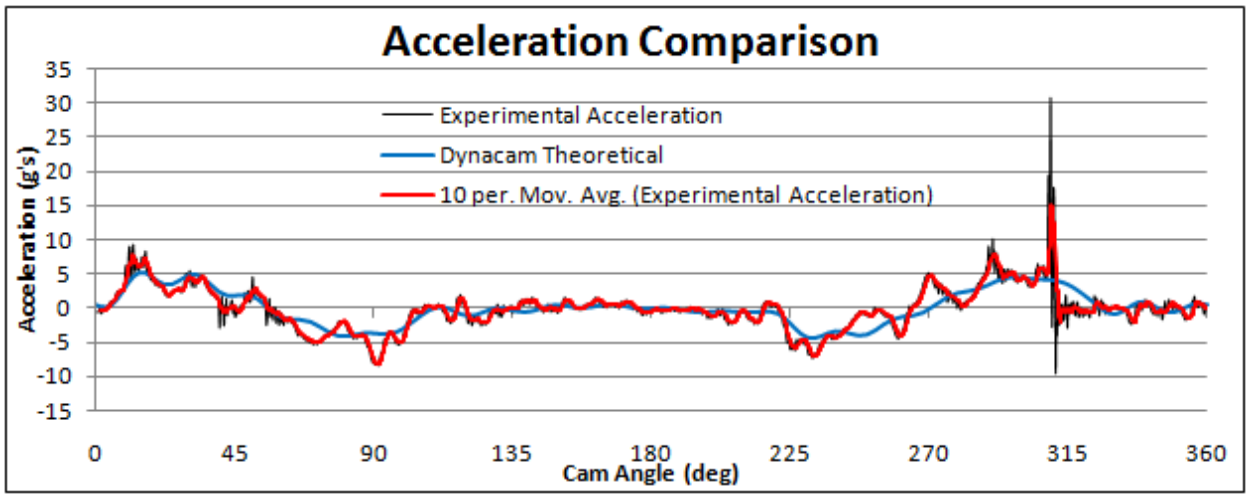

Figure 50: Spline Cam Acceleration Comparison

Using the trapezoidal approximation of integration, the acceleration data for the spline cam was integrated to get the velocity profile. Figure 51 shows the velocity profile of the spline cam after integrating the acceleration data that was collected.

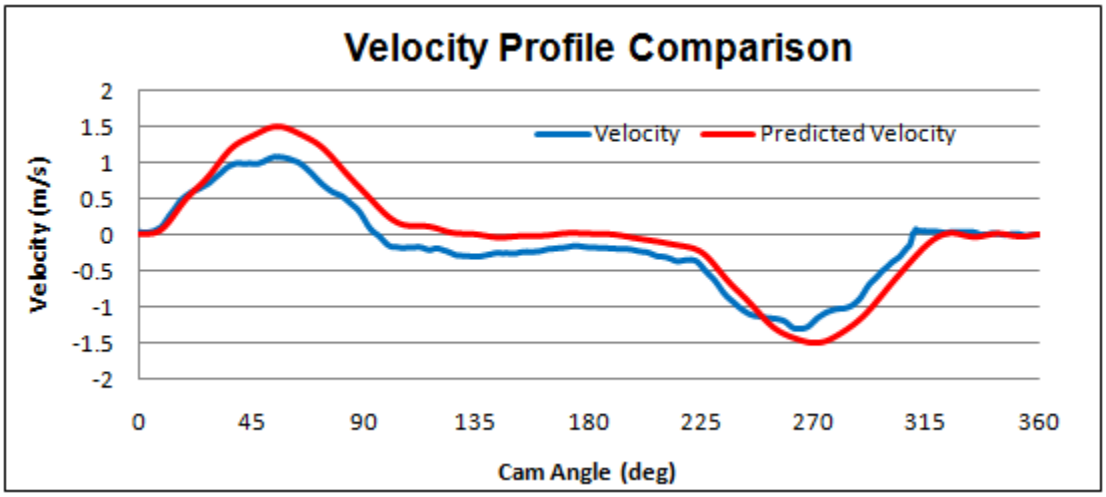

Figure 51: Spline Cam Velocity Profile Comparison

The predicted value from Dynacam is shown in red and the measured velocity of the spline cam is shown in blue in Figure 51. After analyzing the collected data, the redesigned cam does not significantly decrease the impact acceleration and an obvious phase discrepancy was noticed in the velocity profile. We determined that these results were ineffective and that further investigation into the small decrease in impact acceleration and the phase shift of the velocity profile were necessary.

After closer examination of our transfer cam accelerometer data, we determined that a design error had been overlooked. The reason that the accelerometer data we collected didn't show a decrease in impact was because the spline function was designed to control the velocity during cam rise; however, the impact was occurring at the end of the fall. Although we discovered this too late to test a new cam, we did redesign the transfer cam correctly in hopes that further testing can be conducted to resolve the high impact force generated.

When redesigning the final transfer cam, we eliminated the pseudo dwell, dividing the cam into four segments again; however, we still chose to eliminate the modified trapezoidal functions. Mod trap cams tend to have undesirable jerk functions, so instead we implemented a 3-4-5 polynomial function for the rise of the cam. The boundary conditions were the initial and final positions, as well as tying down the velocities and accelerations to zero at the start and end of the rise. We reinserted the original 90° dwell from the original cam. The mod trap cam fall was replaced by a spline function so we could carefully control the velocity. As with all iterations and the original, we kept the final 35° dwell, because this dwell is critical to the timing of the slice bar. Table 9 summarizes the inputs to the Dynacam SVAJ screen for this transfer cam redesign.

Table 9 – Dynacam SVAJ screen input values for the redesigned transfer cam

β	Start	End	Motion	Program	Initial Position	Final Position
115°	0°	115°	Poly	Polynomial	0°	8.143°
90°	115°	205°	Dwell	Dwell	8.143°	8.143°
120°	205°	325°	Spline	B-Spline	8.143°	0°
35°	325°	360°	Dwell	Dwell	0°	0°

The fall of the cam is the crucial component to the cam redesign, as we want to ease the slice bar into the hard stop by controlling the velocity profile. Using a spline function to control the velocity, we first calculated *where* the velocity needed to be controlled. We used the ratio

defined in equation 15 to determine that we wanted to control the velocity when the cam is at a displacement of 0.0895°, at cam angle 311°. At this point (106° into the fall), we applied boundary conditions such that the displacement is 0.0895° and the velocity is at -10 deg/s. We then adjusted the internal knots of the spline to minimize acceleration. The spline function editing screen in Dynacam is shown in Figure 52. Note that the spline function results in a significant increase in jerk; however, this is a tradeoff to control the velocity.

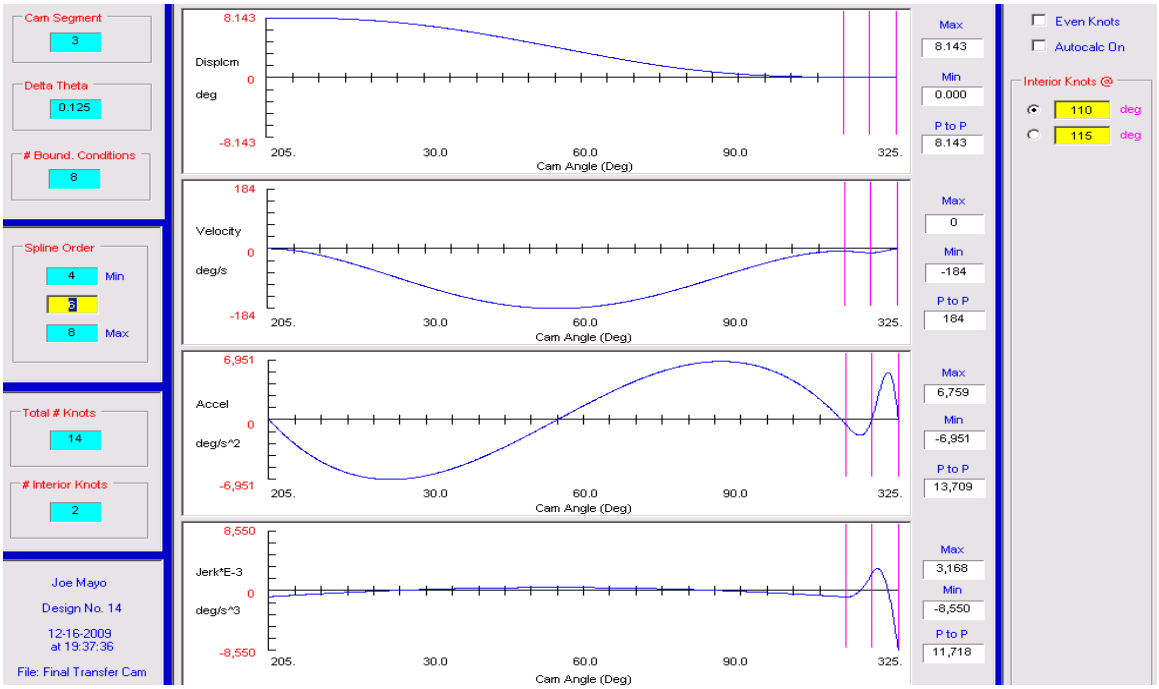

Figure 52: Spline editing screen for the redesigned transfer cam

Although we cannot test this cam design, after adjusting the effective mass and spring constant values, we determined earlier that our dynamic simulation is an accurate model of the system. Figure 53 shows the dynamic simulation of the original transfer cam plotted against out redesigned cam. The peak acceleration decreases by over 500 deg/s^2, from replacing the mod trap rise with a polynomial rise. The mechanical vibration during the 90° dwell is less than that of the original; however, the vibration during the 35° dwell is much larger. This is a tradeoff of having a lower velocity leading into this dwell. If the system behaves as expected, this peak of approximately 6,500 deg/s^2 would be much less than the current impact spike of nearly 75,000 deg/s^2; however, further testing would be required in order to determine if this large acceleration is an improvement. Appendix C shows the drawing for our transfer cam redesign.

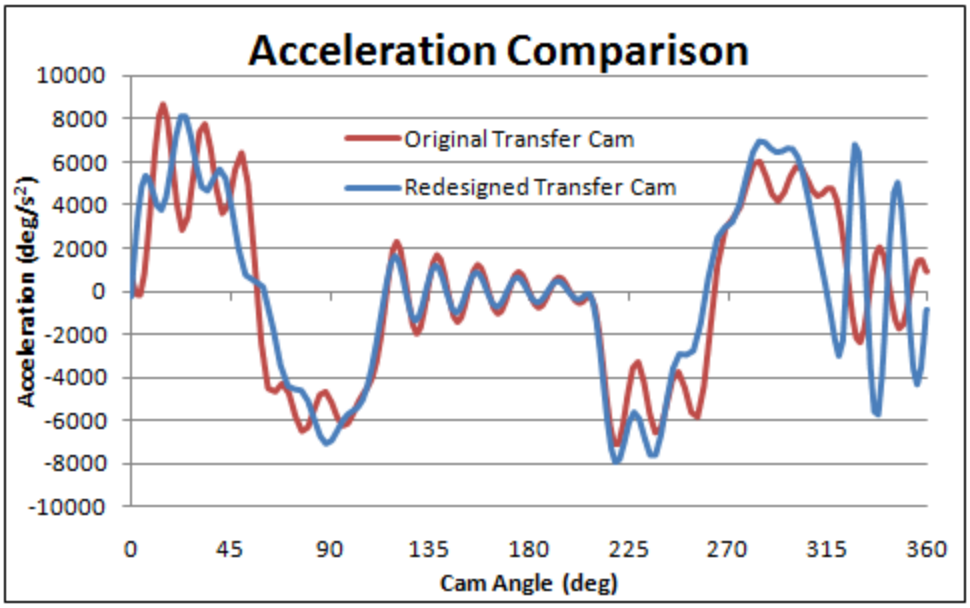

Figure 53: Redesigned v. Original cam dynamic acceleration simulation comparison

Our dynamic simulation suggests that at the point of impact, 311°, the magnitude of the velocity decreases from 31.0 deg/s to 6.6 deg/s. Figure 54 shows the simulated dynamic velocities of the original mod trap cam and our redesigned transfer cam at the point of impact between the slice bar and the hard stop. Note the difference in velocity at the point of impact, circled in the diagram. This decrease in velocity suggests a 79% reduction in the impact force because velocity is directly proportional to impact force.

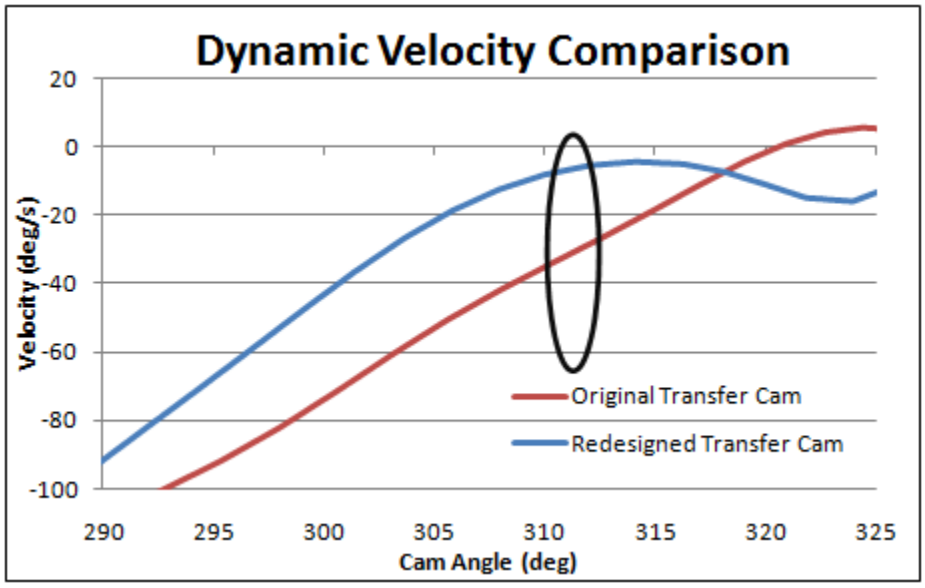

Figure 54: Redesigned v. Original cam dynamic velocity simulation comparison

VII. Conclusions and Recommendations

A high-output product assembly machine currently registers Part A to a known location on an indexing nest by contacting the part against two carbide stops. The contact forces are sufficient to locally deform the edge of Part A. This deformation is undesirable because the crushed edge can lead to loading issues in subsequent product assembly steps in other machines. Part A is placed on the indexing nest at the transfer station and the deformation occurs in the station after this, immediately before Part A is fastened to a support piece. The modification suggested to us by our sponsor was to align the part properly at the transfer station, eliminating product deformation.

The goal for our project was to design a mechanism that would gently register Part A after placement without any deformation. We wanted to ensure that our design fits within the confines of the transfer station such that the alignment mechanism can be removed from the fastening box. We also investigated the dynamics and mechanical vibrations of both cam trains within the system.

We began our project by analyzing the existing conditions at the transfer station of the machine. We recreated the system by building an overall assembly utilizing ProEngineer software and recreated the cams using Dynacam software. We took accelerometer data at the end effecters of both cam trains and compared them to our dynamic simulation. Once our simulation was adjusted to match the dynamics of the system, we could then use our model to predict the outcome of any changes we made to the system. There was a very large impact spike on the transfer cam train from the end effecter hitting into a hard stop. We saw this as an opportunity to reduce the overall mechanical noise on the system by redesigning the cam to gently lower the velocity at which the end effecter approaches the hard stop.

After determining that our simulation was accurate enough to base further predictions off of, we designed a linear cam that could open the jaw of the nest as Part A was placed on it and then gently close the jaw, pushing Part A into an exact location.

In order to make this design easily implementable, we utilized the existing geometry of the end effecter such that our design could simply be attached to the end effecter. We studied the timing of the lift cam, paying particular attention to the velocity of the end effecter during the lift. Because we wanted to control the velocity of the jaw movement, we used the velocity of the pick-up head and the carefully designed cam profile to predict the jaw movement at the roller.

Testing the linear cam on a manually-driven product assembly machine in a prototype lab proved the basic functionality of the linear cam. On a properly set up station, the cam opened the jaw approximately 0.010 inches and gently closed it. We also tested the cam on a production machine, which showed the same results when viewed in high-speed video. This test also incorporated the use of a laser vibrometer to measure the velocity profile of the closing jaw. The data collected during this test matched our predicted velocity, showing that our design would properly align Part A by gently pushing it in place, rather than deforming the product.

We redesigned the transfer cam such that the end effecter would gently approach the hard stop in hopes of reducing the impact force. After the results of our accelerometer tests were inconclusive, we realized an error in our design and redesigned the cam. Due to time limitations, we were unable to test this design; however, our dynamic simulation suggests a 79% reduction in impact force.

Based on our test data, we would like to provide several recommendations regarding both our linear cam design, as well as our redesigned transfer cam.

We recommend that our sponsor conduct further testing of our linear cam. In order to fully test the functionality of our design, a more in-depth test should be conducted which completely eliminates the existing registration mechanism and utilizes ours. This test should include regrinding the carbides on the nests 0.003-0.005 inches such that Part A is correctly aligned on the nest. The station set up should be adjusted in order to move the placement of Part A on the nest forward of the closed carbides by 0.005 inches. This is done by shimming the slice bar base forward in the direction of indexing. The alignment mechanism in the product fastening station should be removed or disabled when running this test. With this set up, we recommend running production at full speed and determining the impact of our design on product quality.

We also recommend that our sponsor manufacture a prototype of our redesigned cam and repeat the accelerometer testing. After replacing the existing transfer cam with our redesigned cam, the machine should be adjusted according to the existing set up procedures to ensure proper alignment. Accelerometer testing should be conducted on the slice bar to measure the impact force. Furthermore, a laser vibrometer measurement should be taken to determine the velocity at impact. This test would require running the machine with the guard open.

Our testing and dynamic simulations show that our linear cam will gently register Part A to a known location, eliminating product deformation. The error in our original cam redesign

demonstrated to us the importance of checking the work of our partners. Our final cam redesign suggests that its implementation will reduce the impact force of the end effecter. We hope that our designs and analysis will allow our sponsor to more efficiently produce their product.

References

"Dowel Pin Tolerance Charts - Engineers Edge." Engineers Edge - Design, Engineering and Manufacturing Solutions. Web. 21 Dec. 2009. <http://www.engineersedge.com/dowel_pin.htm>.

Norton, Robert L. *Cam Design and Manufacturing Handbook.* Industrial Press Inc: New York. 2009.

Norton, Robert L. *Machine Design: An Integrated Approach, 3rd ed.* Industrial Press Inc: Ne York. 2005.

Steffen, John R. Analysis of Machine Elements using Solidworks Simulation 2009. Schroff Development Corporation, 2009. Print.

Yamartino, David E. "Modeling, Analysis and Redesign of Cam-Follower Systems to Increase Operating Speed." Thesis. Worcester Polytechnic Institute, 2004. Print.

Appendix A: Linear Cam Drawing

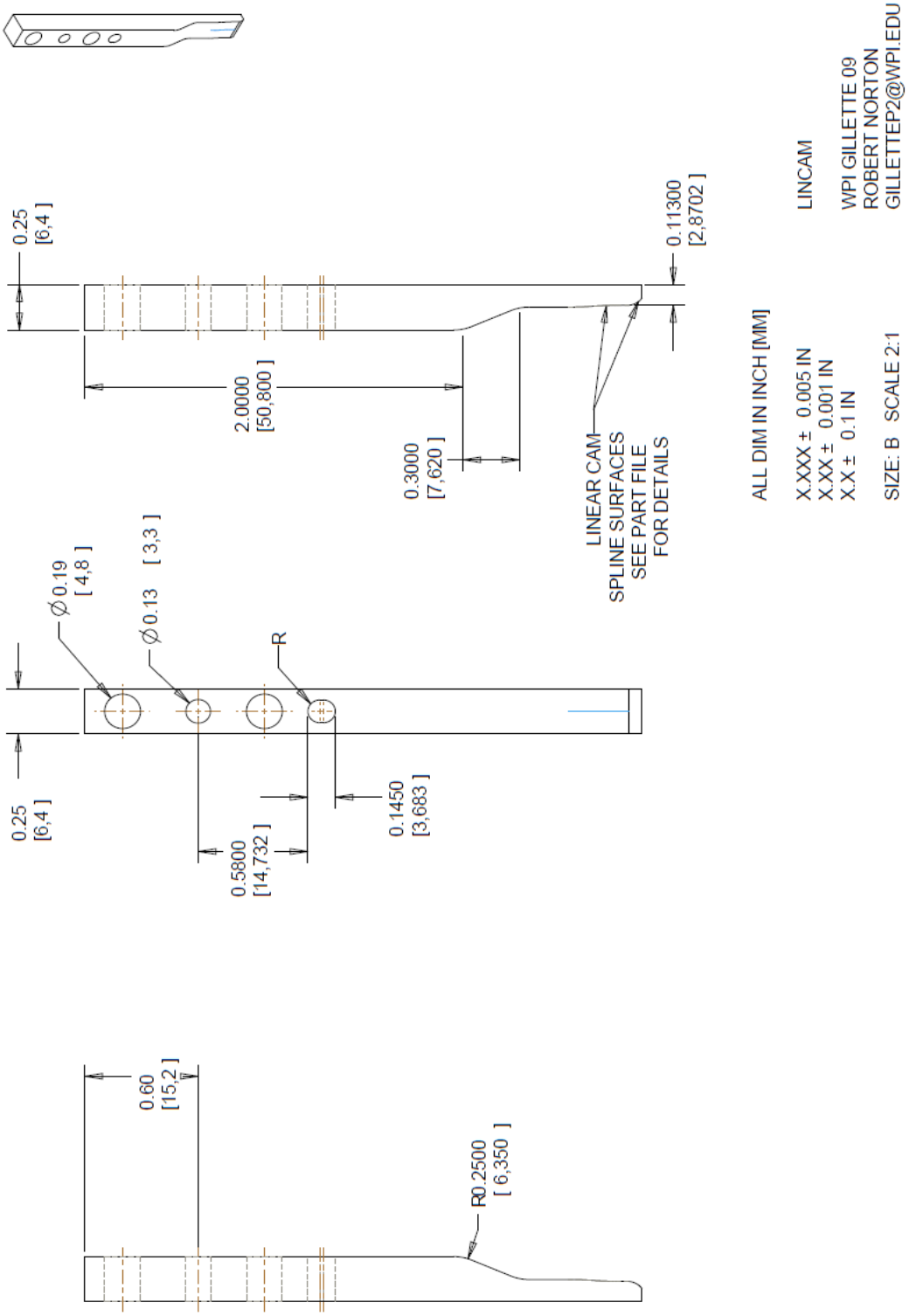

*Not to scale. See drawing file in Appendix F for a scale drawing.

Appendix B: Linear Cam Support Drawing

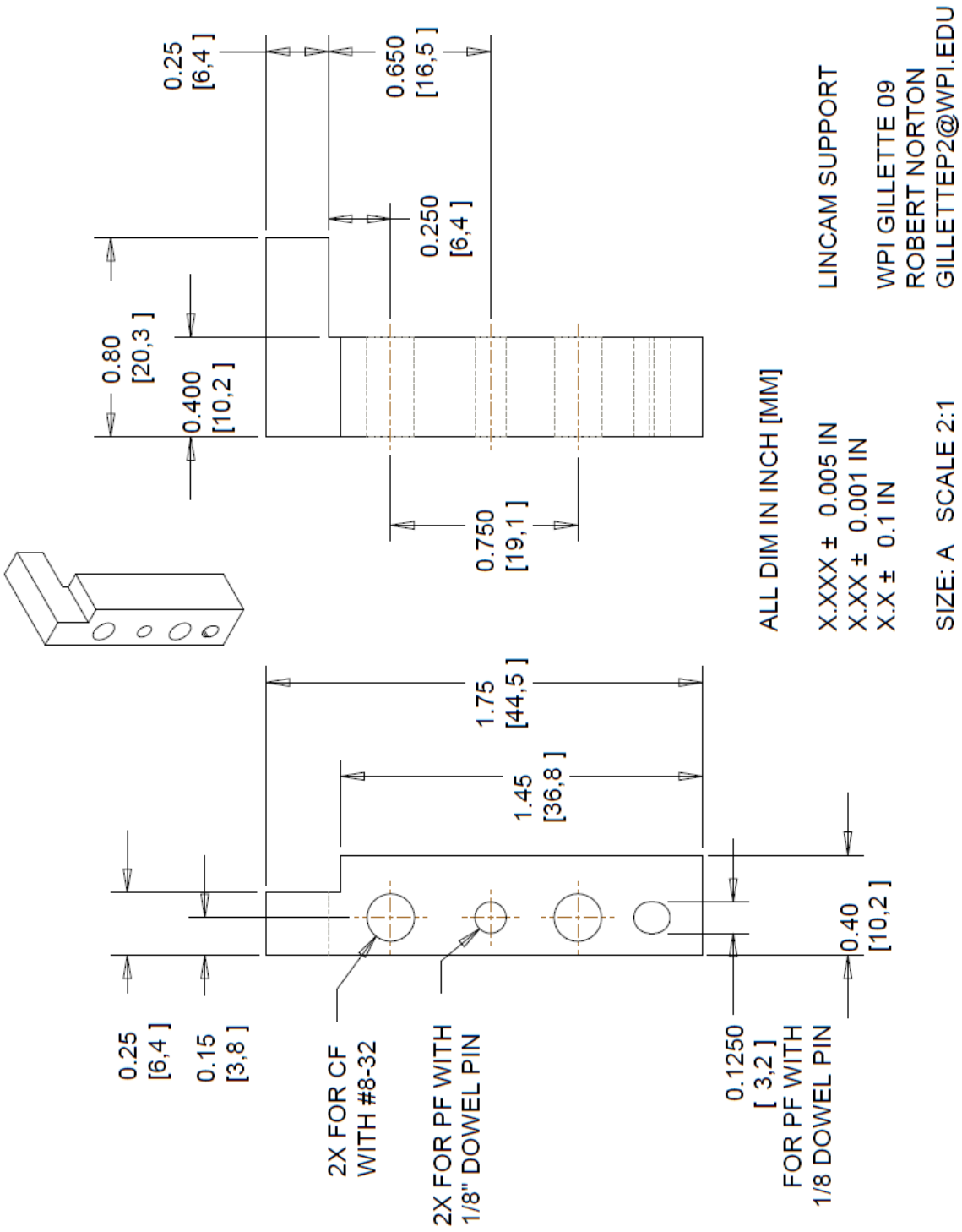

*Not to scale. See drawing file in Appendix F for a scale drawing.

Appendix C: Redesigned Transfer Cam Drawing

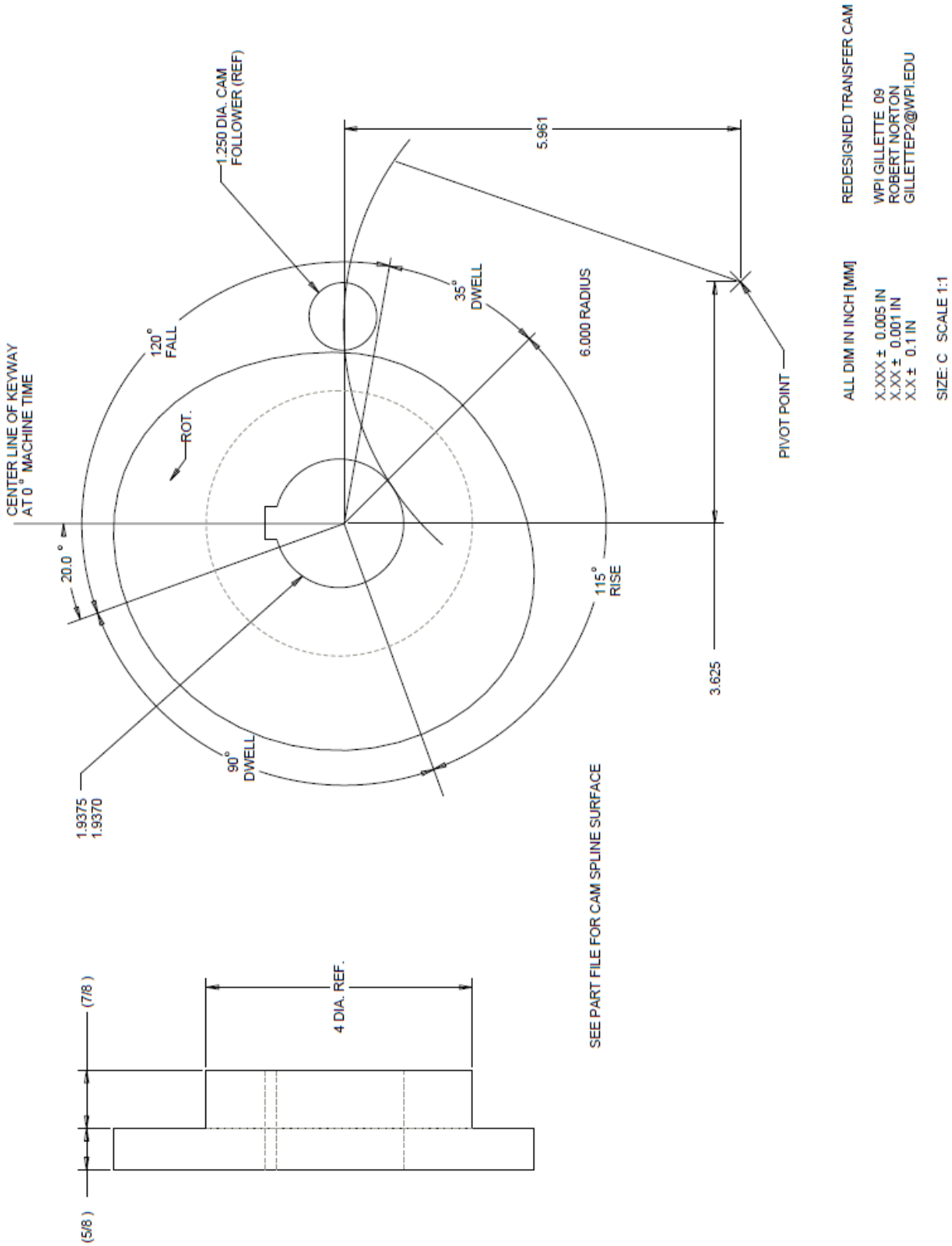

*Not to scale. See drawing file in Appendix F for a scale drawing.

Appendix D: Linear Cam Calculations

Important Dimensions:

$L_1 := .875in = 22.225 \cdot mm$	Length: From the Nest Jaw Pivot to the Flat Top Surface of Jaw (Where Blade Support is Place)
$L_2 := .0095in = 0.241 \cdot mm$	Length: From the Roller Center to the Top Surface of the Nest Where the Locating Pin Enter (Roller is Lower than Surface)
$L_3 := .1in = 2.54 \cdot mm$	Length: Bottom Surface of Linear Cam to the Bottom Surface of Locating Pins (Cam is Shorter than Pins)
$L_4 := .2234in = 5.674 \cdot mm$	Length: From Vacuum with Blade to the Blade Breaker Pad on the Nest (When Locating Pins are .1 in in Holes)
$L_5 := .7375in = 18.732 \cdot mm$	Length: From Front Surface of Vacuum Head to Roller Surface
$L_6 := 1.3365in = 33.947 \cdot mm$	Length: From the Bottom Surface or the Vacuum Head Support to the Bottom Surface of Linear Cam (When Locating Pins are .1 in in Holes)
$L_7 := 168.698deg$	Angle: When the Linear Cam Surface First Touches the Roller
$L_8 := 256.05deg$	Angle: When the Linear Cam Surface Last Touches the Roller
$L_9 := 207deg$	Angle: Start Angle for Dwell
$L_{10} := 233deg$	Angle: Finish Angle for Dwell
$L_{11} := 26deg$	Angle: Length of Lift Cam Dwell
$L_{12} := .2269in = 5.763 \cdot mm$	Length: Distance from when the Linear Cam First Hits Roller to Dwell on the Lift Cam Cycle
$L_{13} := L_{12} + .07in = 7.541 \cdot mm$	Length: Distance from when the Linear Cam First Hits Roller to Dwell on the Lift Cam Cycle with Chamfer Length Included

Linear Cam Motion:

Roller Radius: $r_r := \frac{.2495in}{2} = 3.169 \cdot mm$

Follower Arm Radius: $r_f := .856701in = 21.76 \cdot mm$

X and Y Coordinates: $o := .6715in = 17.056 \cdot mm$

$o' := o + .01in = 17.31 \cdot mm$

$a := .532in = 13.513 \cdot mm$

Start Angle: $\theta := atan\left(\frac{o}{a}\right) = 51.612 \cdot deg$

Finish Angle: $\theta' := asin\left(\frac{o'}{r_f}\right) = 52.702 \cdot deg$

Cam Length: $x := L_{12} \cdot \left(\frac{360deg}{L_8 - L_{10}}\right) = 3.544 \cdot in$ $\quad x = 90.012 \cdot mm$

$r_{lincam} := \frac{x}{2 \cdot \pi} = 14.326 \cdot mm$

$x_c := .07in \cdot \left(\frac{360deg}{6deg}\right) = 4.2 \cdot in$ $\quad x_c = 106.68 \cdot mm$

$\beta_{rise} := L_8 - L_{10} = 23.05 \cdot deg$

Jaw Spring Preload: $10lbf = 44.482\,N$

Jaw Effective Mass: $1.41lb = 0.64\,kg$

Period: $t := .2666s$

Spring Rate: $39.25 \frac{lbf}{in} = 6.874 \times 10^3 \cdot \frac{N}{m}$

Velocity Profile for Lift Cam:

$$\omega_{cam} := 225rpm = 23.562 \cdot \frac{rad}{s}$$

$$ANG := 233deg, 233.125deg .. 300deg$$

$$X(ANG) := \frac{(ANG - 233deg)}{67deg}$$

$C_0 := 0deg$ $C_1 := 0deg$ $C_2 := 0deg$ $C_3 := 60.679425071deg$

$C_4 := -118.91977521deg$ $C_5 := 81.048675212deg$ $C_6 := -18.600425071deg$

$$S(ANG) := C_0 \cdot X(ANG)^0 + C_1 \cdot X(ANG)^1 + C_2 \cdot X(ANG)^2 + C_3 \cdot X(ANG)^3 \ldots + C_4 \cdot X(ANG)^4 + C_5 \cdot X(ANG)^5 + C_6 \cdot X(ANG)^6$$

$$V(ANG) := \left(\begin{array}{l} C_1 \cdot X(ANG)^0 + 2C_2 \cdot X(ANG)^1 + 3C_3 \cdot X(ANG)^2 \ldots \\ + 4C_4 \cdot X(ANG)^3 + 5C_5 \cdot X(ANG)^4 + 6C_6 \cdot X(ANG)^5 \end{array} \right) \cdot \omega_{cam}$$

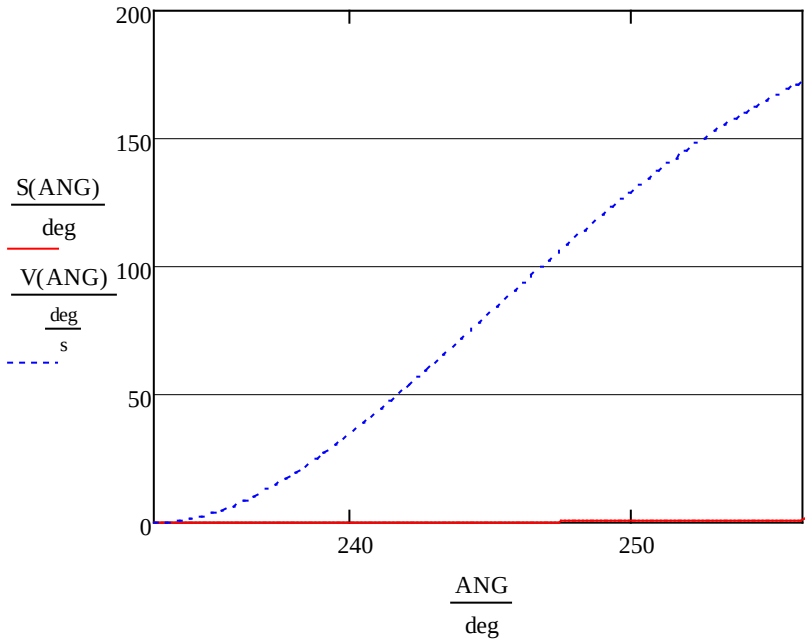

Convert from degrees/sec to inches/sec:

$$V_y(ANG) := V(ANG) \cdot \frac{0.367in}{4.2079deg}$$

Time to Rise:

$$\frac{67deg}{\omega_{cam}} = 0.05s$$

Velocity Profile of Vacuum Slider:

Input:

$r_1 := 5in = 127 \cdot mm$ $r_2 := 9.165in = 232.791 \cdot mm$ $r_3 := 7.961in = 202.209 \cdot mm$ $r_4 := 6.218in = 157.937 \cdot mm$

Find V2:

$$\omega_{bottom}(ANG) := \frac{V_y(ANG)}{r_1}$$

$$v_1(ANG) := (r_2 + r_1) \cdot \omega_{bottom}(ANG)$$

$$\omega_{top}(ANG) := \frac{v_1(ANG)}{r_3}$$

$$v_2(ANG) := r_4 \cdot \omega_{top}(ANG)$$

$r_3 + r_4 = 14.179 \cdot in$

$L_{conrod} := 32.66in$

$O4_x := 5.28in$

$O4_y := 28.74in$

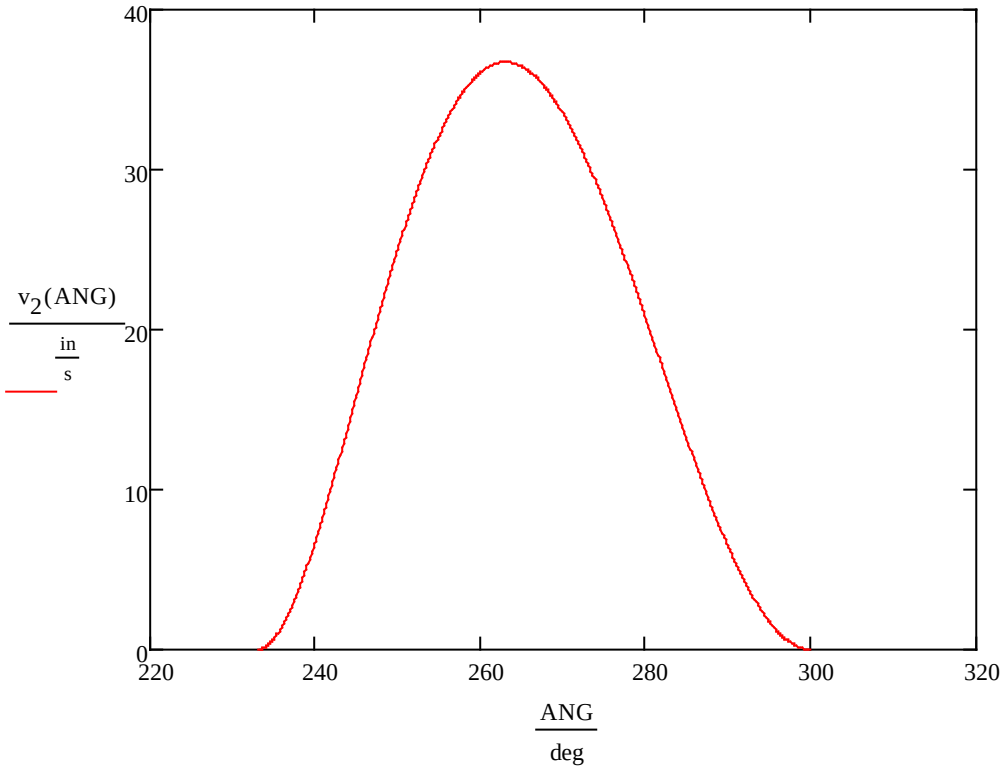

$v_2(256.05deg) = 33.265 \cdot \frac{in}{s}$

Appendix E: Dynamic Impact Force Calculations

Before Redesign

v @ x=8.0535 on the rise

$v := 0.1952286\frac{m}{s}$ $m_e := 7.5kg$ $k := 1600000\frac{N}{m}$

$F_i := v\cdot\sqrt{m_e\cdot k} = 676.292\,N$

$F_i = 152.036\cdot lbf$

Given

$m_e := 11.65kg$ $k := 10200000\frac{N}{m}$ $F_i := 1500lbf$

$F_i = v\cdot\sqrt{m_e\cdot k}$

$\text{Find}(v) = 0.612\frac{m}{s}$

$100\cdot g = 980.665\frac{m}{s^2}$

$100g\cdot m_e = 2.568\times 10^3\cdot lbf$

After Redesign

$\theta = 43.125$

$v := .11053\frac{m}{s}$ $m_e := 7.5kg$ $k := 1600000\frac{N}{m}$

$F_i := v\cdot\sqrt{m_e\cdot k} = 382.887\,N$

$F_i = 86.076\cdot lbf$

$1 - \frac{86.076}{152.036} = 0.434$

$6945N = 1.561\times 10^3\cdot lbf$